Grant agreement no. 312818
SPA.2012.2.2-01 : Key technologies enabling observations in and from space

- Collaborative project -

WP 3 – Interferometer Instrument Technology Development

D3.1 Technical note on the capabilities and performance of the cryogenic test facility and 4 K delay line

Due date of deliverable: month 27

Actual submission date:

Start date of project: January 1st 2013   Duration: 36 months

Lead beneficiary for this deliverable: UL

Last editor: B.Gom, University of Lethbridge (UL)

Contributors:
I. Veenendaal (UL), S. Gunuganti (UL), D. Naylor (UL).

Project co-funded by the European Commission within the Seventh Framework		
Dissemination Level (please refer to the list of deliverables in Annex 1 and complete also		
PU	Public	■
PP	Restricted to other programme participants (including the Commission	
RE	Restricted to a group specified by the consortium (including the	
CO	Confidential, only for members of the consortium (including the Commission Services)	

History table

Version	Date	Released by	Comments
0.1	Jan 16 2015	UL	First draft issue
0.2	Dec 7 2015	UL	Updates for cryostat performance and FTS test results
1.0	Jan 10 2016	UL	Delivered
1.1	Jan 11 2016	UL	Fixed missing references

Table of contents

Acknowledgements

Disclaimer

The content of this deliverable does not reflect the official opinion of the European Union. Responsibility for the information and views expressed in the deliverable therein lies entirely with the author(s).

1 Introduction

1.1 Scope

This document reviews the design, testing and performance of a cryogenic test facility and demonstrator 4 K interferometer delay line development, intended for testing optical components at 4 K and evaluation of cryogenic metrology techniques.

The initial project plan involved retrofitting two existing wet cryostats with closed cycle pulse tube coolers in order to house the required 4 K interferometer and 0.3 K detector system. Additional, external funding was subsequently secured in early 2014 to begin construction of a much larger test facility cryostat which is better suited to housing a cryogenic FTS test-bed. The plan was therefore changed to focus on the component and material tests that could be easily achieved using the smaller 4 K cryostats, and postpone the 4 K FTS tests until the large test facility cryostat is delivered early in 2015.

This report details the current status of the development of the cryogenic test facility and 4 K interferometer. The performance of the current 4 K cryostat and laser interferometer is presented, along with measurements of thermal and mechanical properties of materials relevant to Far Infrared Space Interferometer development. The predicted performance of the 4 K interferometer and 0.3 K detector system are presented, as we finish construction of the large test facility cryostat. The test facility cryostat performance section will be updated when the first tests are complete, and the final version of this document is delivered. This report also includes the initial design of the 4 K FTS mechanism. The performance of the cryogenic FTS will be presented in deliverable D3.6.

1.2 Introduction

Both the interferometry and spectroscopy aspects of FIRI rely on accurate delay lines. For accurate spectroscopic phase retrieval and ghost line suppression, studies have shown that sampling accuracy better than 0.1% of the shortest wavelength is required [1]. Meeting this requirement through optical design and the control of the linear stage is relatively simple on the ground at room temperature, but becomes a substantial challenge in space at cryogenic temperatures. The ongoing activities at the University of Lethbridge in testing of cryogenic delay lines will prove fundamental in identifying key issues in such a design. In this activity a Renishaw differential laser interferometer will be used to evaluate the performance of a cryogenic translation stage mounted in a pulse tube cooled 4 K cryostat. In addition to studying cryogenic metrology issues, the facility will allow the performance of critical components such as beam splitters and filters to be measured in an integrated interferometer and at their nominal operating temperatures.

2   Cryogenic Test Facility

At the beginning of this work, two QMC Instruments wet cryostats with 4 K working volume of ~9L had been retrofitted with pulse tube coolers in order to provide one system for material and component testing at 4 K and one system to house a 0.3 K closed cycle refrigerator and Ge bolometer detector. A new larger volume (~27L) cryostat was under construction to allow much larger mechanisms to be tested at 4 K and ultimately house the 4 K FTS mechanism. The upgrades to the two small cryostats are discussed here along with the current measured performance; the design and predicted performance of the large test facility cryostat is also presented.

2.1   Small 4 K cryostat upgrades

The small volume 4 K cryostat was upgraded with a Cryomech PT415 pulse tube cooler with ~1.5W cooling power at 4 K[2]. New radiation shields were added along with windows and mounts suitable for the operation of a Renishaw differential laser interferometer. A new wiring harness was installed with 68 ETP copper wires between room temperature and the 4 K plate, which can accommodate 15 resistive or diode type thermometers in a low-noise 4-wire configuration.

2.1.1   Shield upgrades

The original cryostat shields were replaced with custom fabricated aluminum 77 K and copper 4 K shields, shown below. Multilayer insulation (MLI) blankets were added to the 77 K shields to reduce thermal loading on the cooler. No load temperatures of ~35K on the first stage and 2.8K on the second stage indicate that the shield and MLI performance is adequate.

Soft 60/40 Sn/Pb solder was used to join the walls of the copper 4 K shield to the bolt flanges, and the entire shield was gold plated to 1μm thickness to minimize the emissivity, but more importantly prevent oxidation of the copper which would impair the thermal contact at the bolted connections. The suitability of soft solder was confirmed by the performance of the 4 K shield.

Both the 77 K and 4 K shields are split at the level of the 4 K plate for easier access to the 4 K work surface. The thermal conductivity of the joint in the shields was measured by placing temperature sensors on the lower section and the shield cap. The temperature difference between the above two sensors was measured to be within 0.5 K.
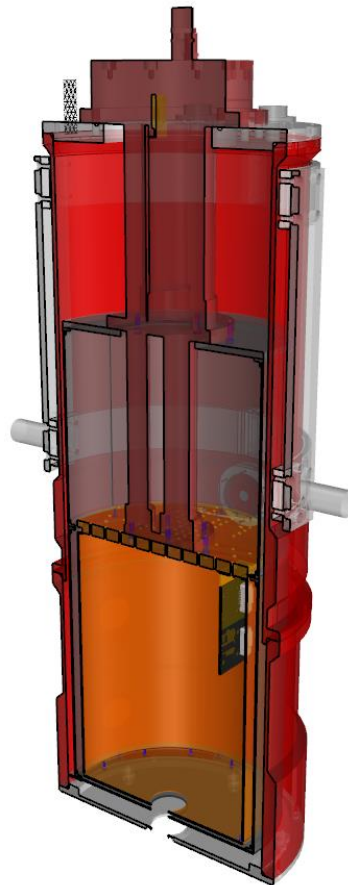
Figure 1 (left) Assembled cryostat with vacuum vessel removed showing upgraded 77 K shield and superinsulation. (right) Cross-section rendering showing inverted system with upgraded 4 K and 77 K shields and bottom-viewing window.

2.1.2 Temperature sensor calibration

A set of Lakeshore Cernox temperature sensors was calibrated using a single factory calibrated sensor [3]. This was done using a platform that was weakly thermally coupled to the 4 K cold plate by stainless steel supports. This allowed for quasistatic measurements of the nearly isothermal sensors during the cool down. By tracking resistance measurements and the temperature readout of the calibrated sensor, calibration curves for temperature as a function of resistance were generated. In total, 11 sensors were calibrated to within 0.2 % of the calibrated sensor over the 4 K to 290 K range; two of these sensors are used for monitoring the pulse tube stages, the others will be used in the large volume 4 K cryostat and FTS mechanism tests. A set of typical calibration curves is shown below, where the large spread in uncalibrated readings can be seen.
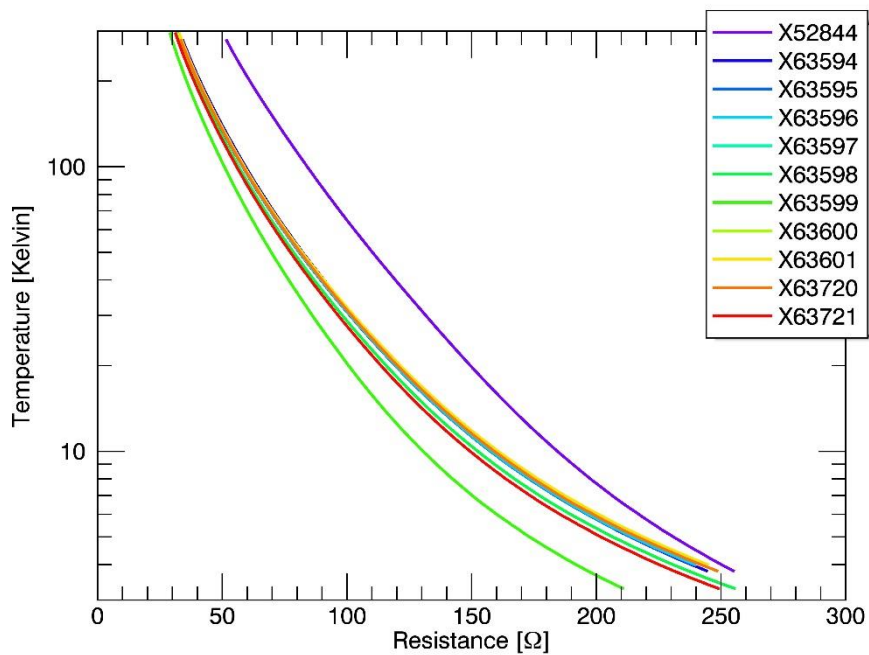
Figure 2. T(R) calibration curves generated in the lab for 11 CX-1010-SD resistance temperature detectors.

2.1.3   4 K pulse tube power loading tests

A resistive heater was placed on the 4 K plate in order to determine the cooling power of pulse tube. The cooler was able to maintain 4.2 K with an electrical load of ~1.1 W, closed to the specified ~1.3 W range allowing for parasitic heat loads in the wiring and shield supports. A typical cool down curve is shown below.

Figure 3. Typical temperatures of the pulse tube cold heads during a cool down of the empty cryostat.

2.1.4   4 K cryostat performance summary

Table 1. 4 K cryostat performance

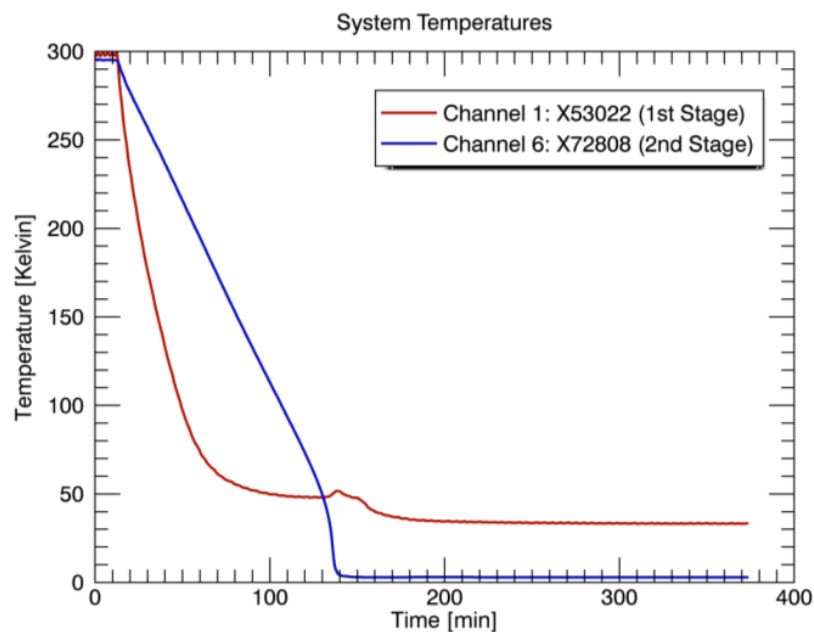|	
4 K work surface diameter	200 mm
4 K work surface volume	9 L
Pump out time	~3 hrs.
Cool down time from 300 to 4 K	2 hrs.
Warmup time	< 8 hrs.
Cooling capacity at 4.2 K	~1.3 W
Thermometry channels	15
Thermometry calibration accuracy	~0.2%

2.2   0.3 K detector cryostat design

The second wet cryostat was upgraded with a Cryomech PT403 pulse tube cooler in order to house a 0.3 K closed cycle fridge and bolometric detector [4]. The PT403 cooler provides ~0.25 W at 4.2 K, which is just sufficient to cool a Chase Cryogenics gas-light He10 closed cycle ^{3}He-^{3}He-^{4}He 0.3 K refrigerator (see Figure 4)[5]. The pulse tube cooler includes a vibration isolation framework which isolates the pulse tubes from the 4 K cold surface, which is critical to minimize microphonic pickup in the high-impedance bolometer signal.

2.2.1 ^{3}He- ^{3}He-^{4}He fridge mount

The three cold heads on the ^{3}He-^{4}He fridge are expected to run at about 220 mK (^{3}He ultra-cold head), 290 mK (^{3}He intermediate-cold head), and 850 mK (^{4}He buffer head) under zero load conditions. The run time is expected to be at least 20 hours under thermal loads of around 2-3 μW on the ultra-cold ^{3}He head, 50 μW on the intermediate-cold ^{3}He head and 200 μW on the ^{4}He buffer head. The intermediate-cold head and ultra-cold head will run beyond 20 hours and during this time the ^{4}He buffer head can be recycled independently [6].

The maximum power required for the first cycle ^{3}He-^{4}He fridge on its 220 mK head pump heater, 290 mK head pump heater and 4 K head pump heater are 1.33 W, 1.44 W and 2.88 W respectively. During the first cycle, all the pump heaters are turned on for ~30 minutes and then turned off once the liquefaction of ^{3}He and ^{4}He has been achieved. Lower power can be applied to the heaters but the tradeoff is a longer cycling time. The corresponding heat switches conduct only 5 mW, 4 mW, and 31 mW, respectively, when the fridge is running at base temperatures. The maximum power requirements for re-cycling the fridge once cold is the same as mentioned above for the first cycle, but with reduced duration for the pump heaters (6 to 20 minutes) [6].

The ^{3}He-^{3}He-^{4}He fridge is mounted to the 4 K plate in the detector cryostat by three ½" diameter oxygen free high conductivity (OFHC) copper rods and bolt flanges (See Figure 4). OFHC copper is required in order to maximize the thermal conductivity to the 4 K plate and prevent the fridge from overheating during the helium recycling sequence. A total thermal conductance of ~1 W/K is provided by the rods, which maintains the refrigerator base plate below ~5.8 K while the heaters are active and ensures a rapid

return to base temperature when the pumps are activated, thereby minimizing the fridge recycling time
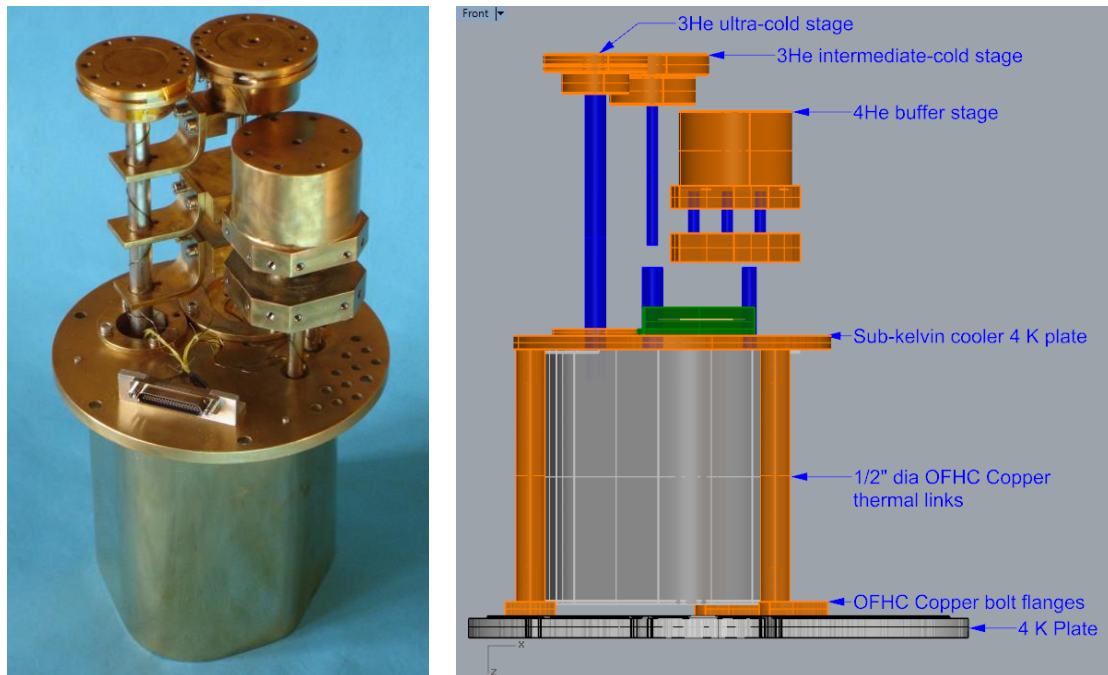

Figure 4 ^{3}He3he-^{4}He fridge (left). Thermal links between fridge and 4 K plate (right).

2.2.2 Shield upgrades

The detector cryostat design calls for a split in the 77 K and 4 K shields at the same level as the split in the outer vacuum vessel (OVC), to provide easy access to the 4 K work surface. The feasibility of using a split shield was confirmed by measuring the temperature difference between the 4 K shield and removable shield cap inside the existing PT415 4 K test cryostat (See Section 2.1.1). The temperature differential was acceptable at <0.5 K.

The mating flanges of the two 4 K shield sections also serve as a mounting locations for 3 fiberglass support struts between the 4 K and 77 K shields, designed to minimize stress on the pulse tubes from the large 4 K copper mass when the cryostat is tipped on its side. The thermal conductance of the struts is negligible at ~12 mW. The mating rings are designed with nested grooves to minimize stray light infiltration.

The top and bottom 4 K shields have been manufactured and will be gold coated before being installed in the cryostat.
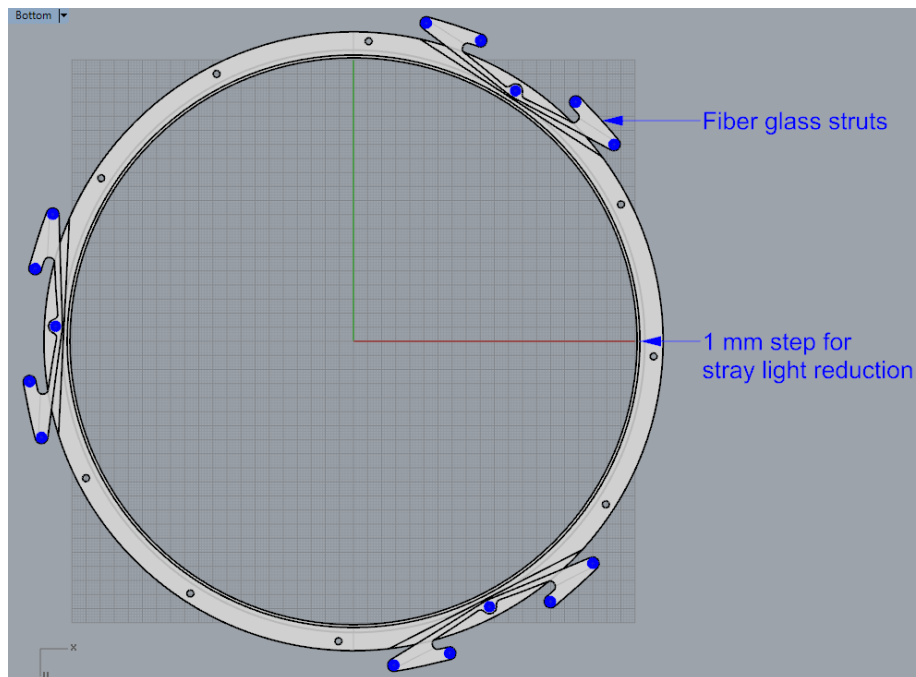
Figure 5. Mating flange between the two 4 K shields.

Figure 6. One section of the 77 K shield with MLI blanket.

In order to control the background power reaching the detector in a quantifiable manner a variable aperture cold field stop is used. An adjustable 4 K iris is mounted in a copper block immediately in front of a field lens and attached to the 4 K top shield (see Figure 6). The HDPE field lens was designed and manufactured in house to fit the iris mount

and acts to reimage the pupil stop of the laboratory FTS onto the detector feedhorn aperture. As a result of this work optimal lathe turning parameters for machining HDPE and high purity copper have been established for future optics fabrication. Thermal grease will maximize the thermal conductivity between the lens and the mount, in order to minimize thermal emission seen by the detector.
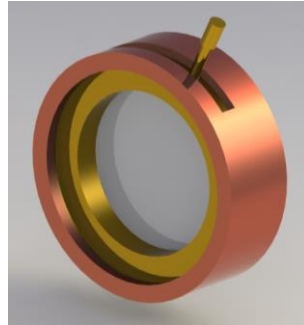
Figure 7. Adjustable field stop iris and HDPE lens in copper mount.

2.2.3   4 K Wiring

The detector circuitry, thermometry, and 0.3 K refrigerator require at least 90 wires between the 4 K plate and the OVC connectors. The wire material is determined in Section 2.2.4. The cryostat OVC connector plate was designed for 5 LEMO connectors, each with at least 20 conductors [7]. 5 braided ribbon cables, each with 12 twisted pairs will be used. Slots in the 4 K and 77 K plates allow the braids to pass through, with clamps providing heat sinking and blocking stray light (see Figure 8). A cap covers the end of each slot and the remaining gap between the 4 K plate and the shield flange is filled with Eccosorb to reduce stray light [8].

Figure 8. Slots in 4 K plate for heat sinking the wiring whereas 77 K plate has the similar slots and heat sinking plates.

The 4 K plate also has a 1 mm step on the outer edge just inside where 4 K shield is connected to reduce stray light from entering the 4 K volume.

Figure 9. 4 K plate showing the copper heat sink clamps for up to 3 pairs of ribbon cables, and stray light caps.
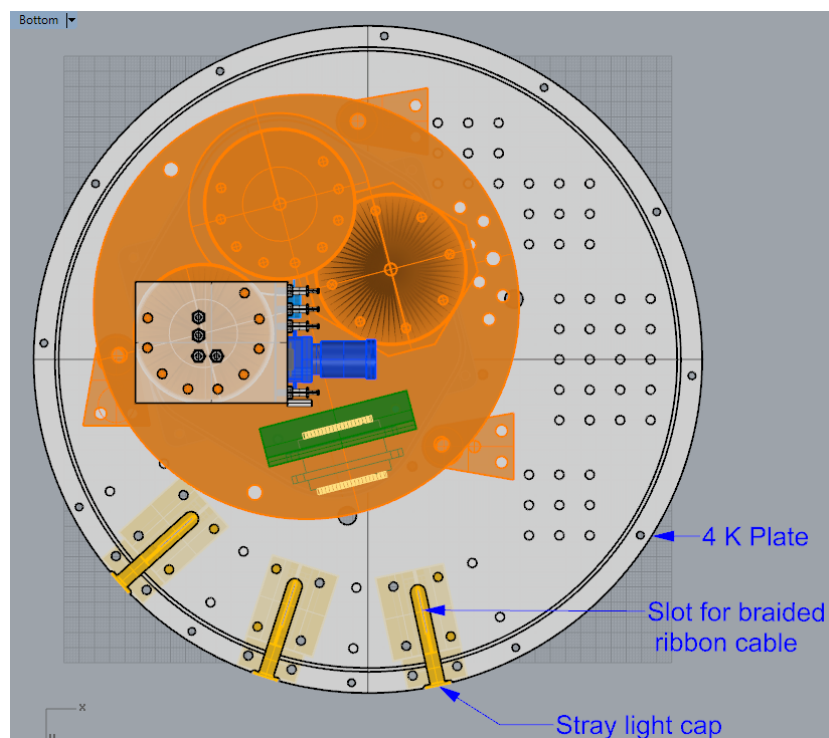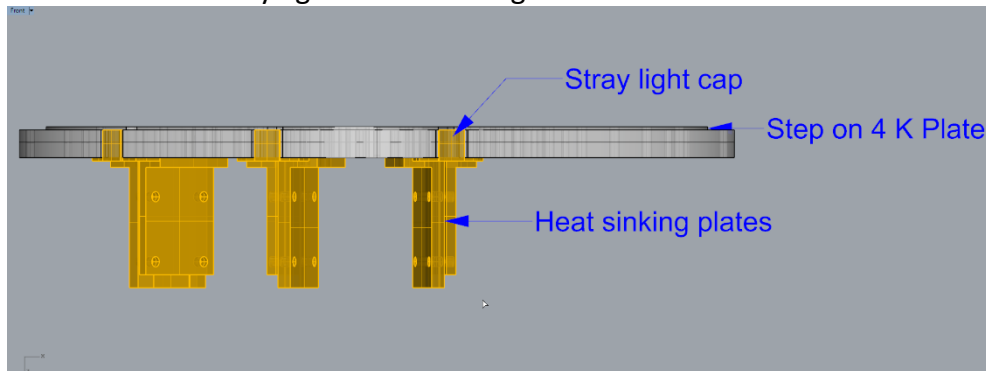
2.2.4 Thermal calculations

Thermal loading calculations are currently underway to determine the proper wire alloy, length and thickness to use in the wiring harness between 0.3 K and 300 K. Manganin and Constantan are commonly used below 1K due to their low thermal conductivity [9], but Beryllium Copper also has suitably low thermal conductivity and is easier to solder [10]. The total conductance for the various alloys and available wire gauges shows that while pure copper is unsuitable, 36 AWG BeCu wires would meet the thermal loading requirements for the 8 wires between 4 K and 0.3 K.

Table 2. Calculated 0.3 K cryostat wiring thermal conductance

Wire Alloy (36 AWG)	255 mK stage load (µW)	330 mK stage load (µW)	890 mK stage load (µW)
Manganin	0.001	0.025	0.317
Constantan	0.002	0.033	0.534
BeCu (C17200)	0.013	0.208	1.408
BeCu (C17510)	0.054	0.831	7.076
Copper	2.9	45.8	400
Total Fridge Capacity	**4**	**50**	**200**

Similarly, it was determined that a combination of Cu and BeCu ribbon cables would be suitable for the 4 K to 77 K connections, requiring ~18 mW of the 250 mW total cooling capacity of the pulse tube cooler at 4 K. Copper wires will only be used for the high current heater lines where the electrical resistance of BeCu is too large. Between the 77 K stage and the 300 K OVC, these ribbon cables only consume ~41 mW of the 10W available cooling power (see Table 3).

The radiative heat load from the shields, MLI (multi-layer insulation), fiber-glass struts, and OVC of the detector cryostat on the 4 K and 77 K cold plates was calculated based on surface area and emissivity, as given in the table below [11].

Table 3. Calculated 0.3 K cryostat thermal loads

Stage	Description	Heat Load	Total heat load	Cooling capacity
0.255 K	Wiring load	0.013 µW	0.086 µW	4 µW
	Radiation load	0.073 µW		
4 K	Wiring load	0.0182 W	0.042 W	0.25 W
	Radiation load	0.0119 W		
	Fibre glass strut load	0.0115 W		
77 K	Wiring load	0.0412 W	0.478 W	10 W
	Radiation load	0.437 W		

2.2.5 Expected performance

The estimated cool down time of the detector cryostat from room temperature to 4 K is approximately 6-8 hours. The ^{3}He-^{3}He-^{4}He fridge will take approximately 70 minutes to bring the temperature of the detector to 0.255 K.

The frequency coverage of the 0.3 K bolometric detector will be 2 to ~100 cm^{-1}, determined by the combination of the low pass filter on the 77 K shield and optional bandpass filter on the detector feedhorn. The low-pass filter rejects thermal IR and reduces loading on the 4 K and 0.3 K stages.

The expected cutoff frequency for the detector is ~100 Hz which is sufficient for FTS modulation frequencies in the spectral region between 2 cm^{-1} and 40 cm^{-1}. The typical NEP of the bolometer element is ~5×10^{-16} W/$\sqrt{\text{Hz}}$, enabled by the low thermal conductivity of the bolometer element and carefully designed fully differential detector, preamplifier and data acquisition electronics [12].

Table 4. Predicted 0.3 K cryostat performance

Pump out time	~3 hrs.
Cool down time from 300 to 4 K	6-8 hrs. (estimated)
Cool down time from 4 K to 0.3 K	70 min. (estimated)
0.3 K fridge recycling time	~90 min.
Warmup time	< 8 hrs.
Cooling capacity at 4.2 K	0.25 W
Cooling capacity at 0.3 K	4 µW
Thermometry channels	17
Thermometry accuracy	~0.2%
Detector NEP	~5×10^{-16} W/$\sqrt{\text{Hz}}$
Filter bandpass	2 to 40 cm^{-1}

2.3 Large test facility cryostat design

As noted above, additional external funding was secured early in 2014 for the purchase of a large volume test facility cryostat. Testing of the small volume 4 K cryostat and design of the 0.3 K detector cryostat upgrades continued in parallel with the design of the large test facility cryostat so that the work package would not be delayed while waiting for delivery of the larger system which took place in early 2015. Since the large

cryostat affords roughly 3 times the usable 4 K work volume of the existing cryostat and features viewports in much more suitable locations, the 4 K FTS design was tailored for use exclusively in the large cryostat. This allows more flexibility in the optical design, and also opens the possibility of mounting the 0.3 K detector and low temperature blackbody source within the same low-background 4 K enclosure.
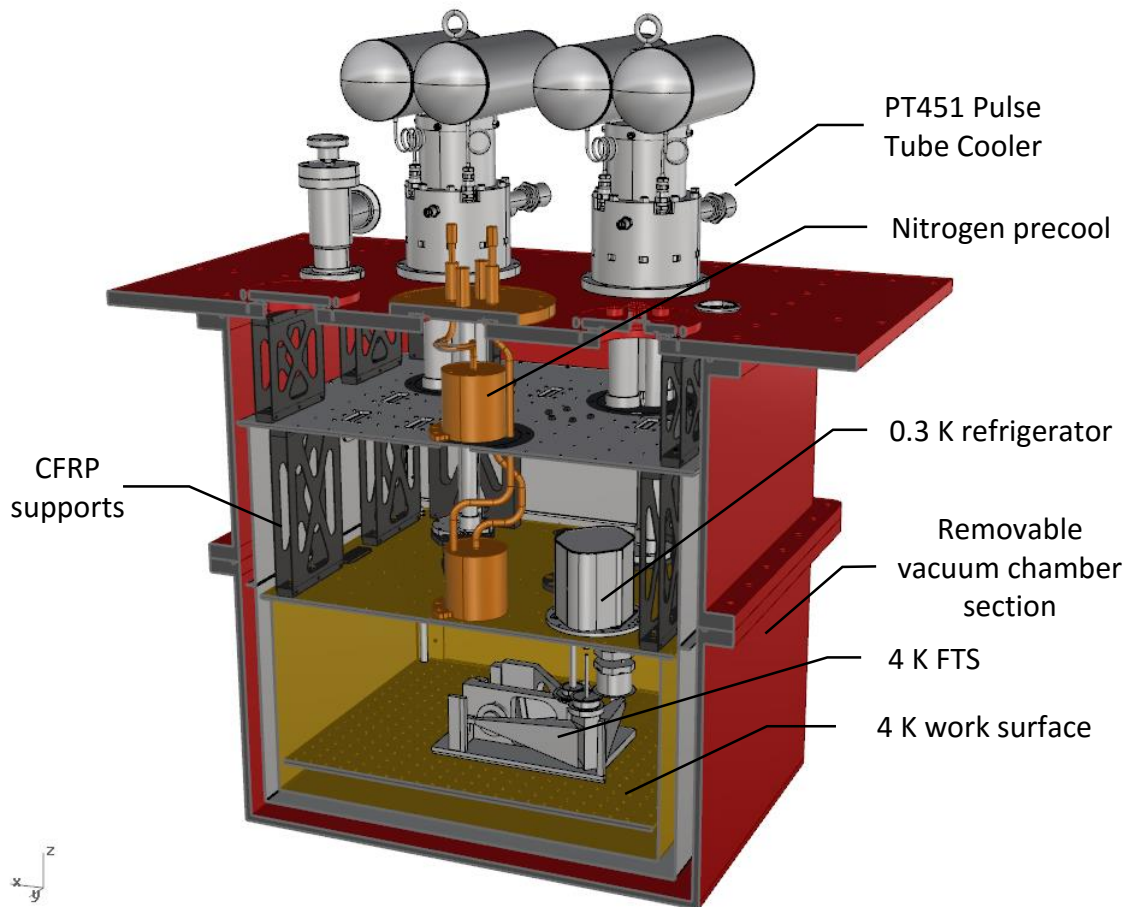
Several designs for the large test facility cryostat were considered, beginning with the original design proposed for testing of the SAFARI optical delay line (see Figure 10). The original design included a horizontal cylindrical vacuum vessel that would provide maximum access to the 4 K work surface, but unfortunately was proven by FEA simulations to be insufficiently stiff to provide the required low-vibration platform for interferometer testing.
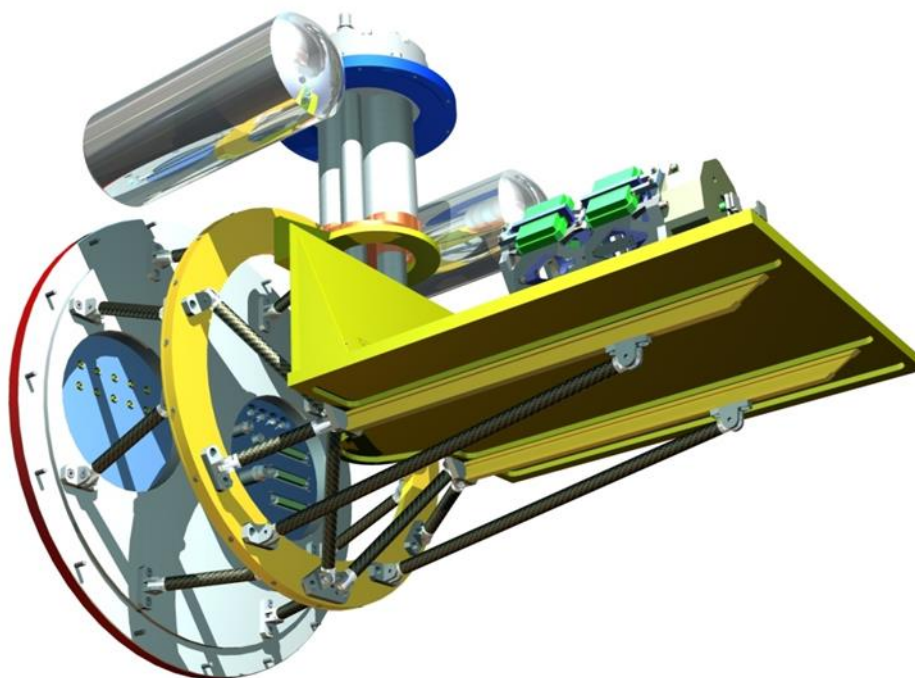
Figure 10. Internal components of the original cryostat design, with horizontal 4 K work surface supported by cantilevered CFRP struts and cooled by a single PT415 pulse tube cooler.

A vertical design was chosen, with rigid CFRP plates used to connect the 4 K, 45 K and room temperature stages, due to the increased mechanical stiffness. Two Cryomech PT415 pulse tube coolers can be used to provide maximum cooling power, with flexible braided thermal links connecting the pulse tubes to the cold structures in order to decouple mechanical vibrations. Due to budget constraints, only one cooler has been installed for initial testing. Since a vertical design was required, the vacuum chamber is split at the 4 K level and the entire system is suspended by the top plate from a support framework. The lower section of the OVC can be removed, along with the lower sections of the radiation shields, to give full access to the experimental volume. The 4 K stage consists of two horizontal copper plates. The upper plate serves as the mounting point for the pulse tubes, nitrogen precooling heat exchanger, wiring harness, and 0.3 K refrigerator. The lower plate serves as a more convenient mounting surface for

experiments, with easy access once the side plate(s) of the 45 K and 4 K shields are removed.

PT451 Pulse Tube Cooler

Nitrogen precool

0.3 K refrigerator

CFRP supports

Removable vacuum chamber section

4 K FTS

4 K work surface

Figure 11. Cutaway view of the large test facility cryostat final design.

Electrical connections are provided on reconfigurable plates on the top of the cryostat, with ~96 conductors wired to the 4 K stage. 36 wires are required for the operation of the 0.3 K refrigerator; the remaining wires are sufficient for thermometry and control of the FTS mechanism.

Two large viewports along with smaller viewports are provided on the long sides of the removable vacuum chamber as shown in Figure 12, allowing optical windows of up to 150 mm diameter to be installed. Three smaller flanges are provided with one each on the short sides and the bottom side of the chamber for additional windows or mounting the Renishaw laser interferometer.

Figure 12. Outer vacuum chamber for the test facility cryostat, showing one of the large aperture viewports and two smaller 50mm diameter ports. These viewports are mirrored on the rear side, and three additional 50 mm diameter ports are located on the short sides and bottom of the vacuum chamber for the Renishaw differential interferometer.

2.3.1 Thermal loading calculations

A key motivation for the construction of the large volume cryostat was to provide quick turnaround time for experiments. The time required to warm up the system, access the 4 K components, and cool the system back down must be minimized. A practical limit of 12 hours for the cool down time allows the system to be cooled overnight. With a fixed cooling power, the mass of the low temperature structures must therefore be minimized while still ensuring that the mechanical stiffness is high enough to keep any mechanical resonances well above the ~100 Hz frequencies of interest for the interferometry measurements.

The system consists of ~12 kg of copper and ~5 kg of aluminium in the first stage, and ~36 kg of copper in the second stage. This represents ~1.8 MJ of energy to cool the first stage from 300 K to 45 K, and ~2.8 MJ of energy to cool the second. A target of 3 hrs for the precool stage corresponds to ~166 W and ~262 W for the first and second stage power requirements. Since two PT415 pulse tubes provide a total of ~160 W at 70 K or ~84 W at 40 K for the first stage and ~3 W at 4 K for the second stage, the two pulse tubes should be sufficient for the precooling phase on the first stage, but extra cooling power is required for precooling the second stage. A liquid nitrogen precooling system is therefore included in the cryostat, which works in parallel with the pulse tubes to

provide an extra ~500W of cooling power above 77 K with a liquid consumption rate of ~ 8 L/hr. Heat exchangers are connected to both stages and are fed with a single liquid nitrogen supply line.

The wiring harness consists of 84 conductors between the outer vacuum vessel and the 4 K work surface. 20 AWG 34 copper wires, 20 AWG 36 phosphor bronze wires, and 44 AWG 39 copper wires provide a good balance of current capacity with parasitic heat loading of ~72 mW on the first stage and ~41 mW on the second stage, well within the cooler budget.

The first stage radiation shields include multilayer insulation blankets, and with a surface area of ~ 2 m^2 there is a heat load of ~ 3 W. The 4 K shields present a 60 mW load to the second stage. The CFRP support struts that suspend the first and second stage structures also represent a parasitic heat load of ~3.9 W on the first stage and ~0.3 W on the second. The total thermal load on the first stage is predicted to be ~ 7 W on the first stage and ~0.4 W on the second stage. This is small relative to the conductive heat load produced by the internal energy of the metal in the system, and therefore does not significantly affect the cool down times. This also allows the system to be maintained at 4 K with only one pulse tube running, which will reduce vibration and also allow contingency for cooler failures.

Warming the system rapidly back up to room temperature will be accomplished by backfilling the system with helium gas (once all components are above 4 K. Thermal conductivity of helium at ~1 mbar is large, and the available warming power is limited by the surface area of the OVC while maintaining the OVC O-rings and windows above the freezing point. A warmup time on the order of a few hours should be achievable, although in practice the system will likely be left to warm up overnight.

2.3.2   4 K test facility cryostat performance

The predicated and actual performance parameters of the Test Facility Cryostat are given in the following table. The 4 K work volume of the Test Facility Cryostat is 580 mm x 480 mm x 250 mm (WxDxH).

Table 5. Test facility cryostat performance.

	Predicted	**Actual**
Size	1.5 x 0.75 x 2 m	1.5 x 0.75 x 2 m
4 K Volume	580 x 480 x 250 mm	580 x 480 x 250 mm
MLI	30 layers	12 layers
Pump out time	4 hrs.	3.5 hrs.
Precool time from 300 K to 77 K	3 hrs.	4 hrs.
Cooldown time to 4 K	12 hrs.	17 hrs.
Warmup time	24 hrs.	38 hrs.
Cooling capacity at 4.2 K	3 W (total) with 2 PTC	250 mW (residual) with 1 PTC
Wires to 4 K	96	84
Thermometry channels	Up to 16	15
Viewports	2x 150mm dia., 2x 50mm dia. minimum	2x 150mm dia., 7x 50mm dia.

2.3.3 Cooling Time

On April 28, 2015, the Test Facility Cryostat was successfully cooled for the first time. Thermometers were located on the 4K and 45K plates and pulse tube cold heads and one was placed on the warm end of the 45K shields. The total cooling time with a full liquid nitrogen precool was found to be approximately 9 hours.
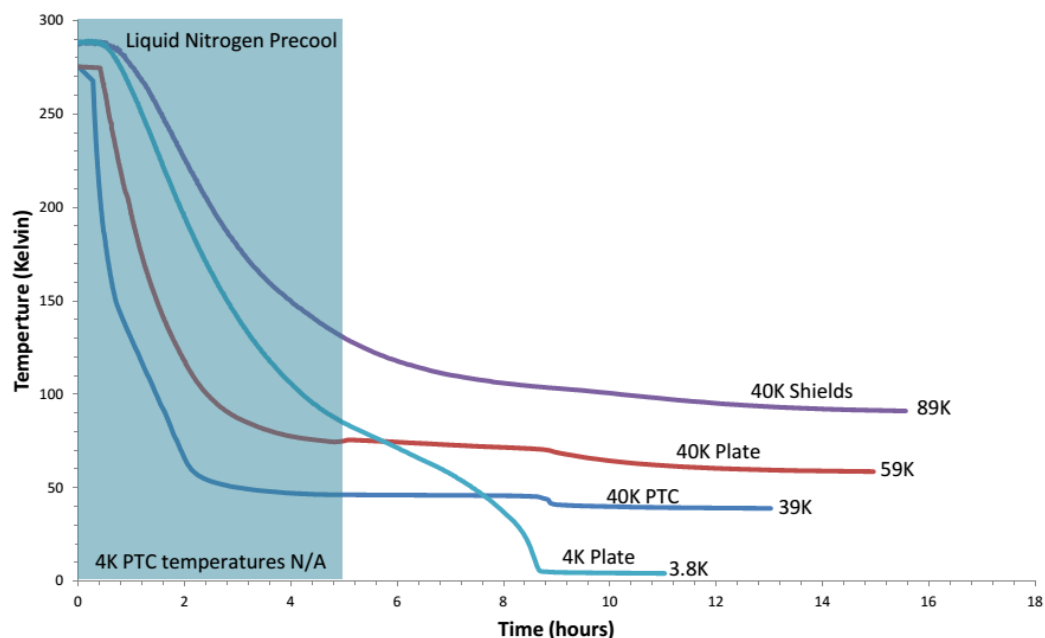
User: University of Lethbridge, Ian Veenendaal
Manufacturer: Quantum Technology Corporation, Yan Pennec
Date: April 28, 2015

Figure 13. The first successful cool down of the Test Facility Cryostat. Precooling was accomplished by a continuous flow of liquid nitrogen from a 50L pressurized (20 bar) dewar for 5 hours. Total cooldown time was ~9 hours to 4K.

The thermal map of the Test Facility Cryostat was established in the subsequent cool downs by placing temperature sensors at various locations on both 4 K and 45 K stages. These measurements were performed without liquid Nitrogen precool and using a single pulse tube cooler. The temperature of the top and bottom plates in the 4 K work volume has reached 4.0 K after around 24 hours, whereas it took another ~6 hours for the shield temperatures to come to an equilibrium at slightly higher than their expected temperatures.
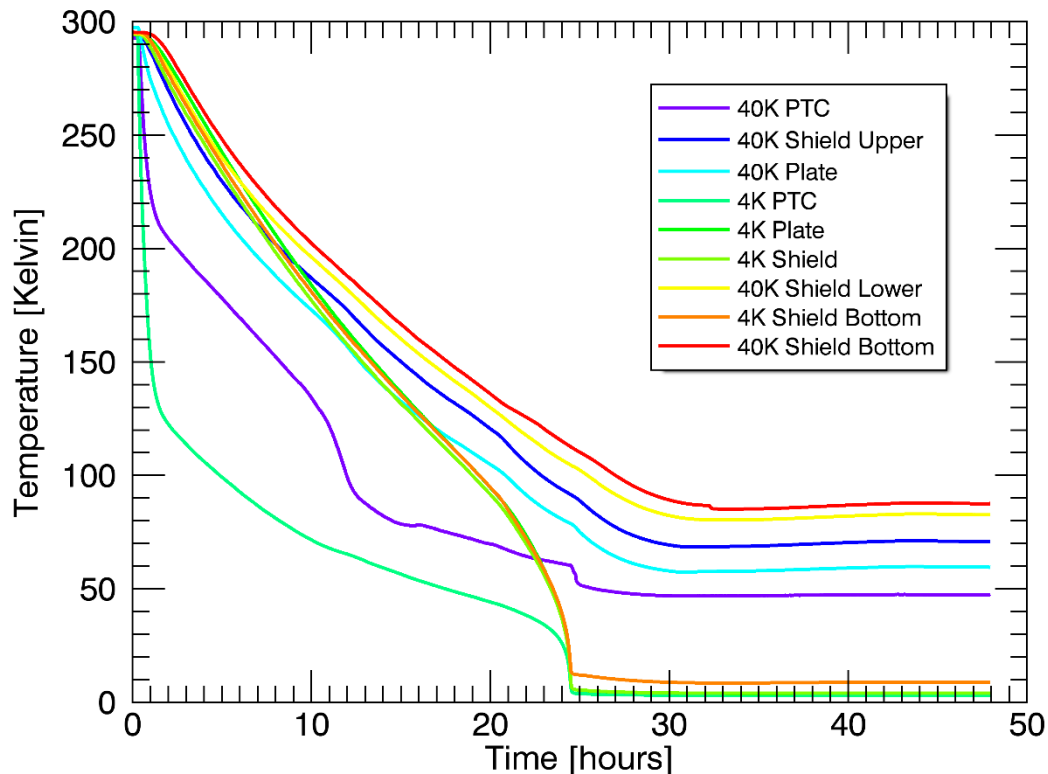

Figure 14. Temperature logs for cool down of the empty Test Facility Cryostat without precooling.

2.3.4   Shield Temperatures

The ultimate warm shield temperature of 89K (Figure 13, Figure 14) was achieved using multiple layers of aluminized Mylar insulation or multilayer insulation (MLI). The number of layers was kept to a minimum to keep the overall thickness of the MLI to a minimum. This was done to lower the chances the MLI would snag in the seams between the shields or vacuum chamber on assembly and also to avoid the MLI from touching the inner wall of the vacuum chamber, causing unnecessary parasitic heat conduction. 8-12 layers of MLI were found to be sufficient to keep the 45K shield temperatures below 100K at the warmest point.

2.3.5 Cooling Power

Although the pulse tube cooler has a specification of 1.5 W cooling power at 4.2 K, most of this power budget is consumed by parasitic radiative heat loading from the shields and conduction through the internal wiring and mechanical structure. The net cooling power at the 4 K plate was measured directly and compared to results from thermal modelling. A 5 W resistive heater was mounted and thermally coupled to the edge of the 4 K plate. Two thermometers were placed on the plate; one thermometer sat near the heater and the other sat on the opposite edge of the plate. The heater was wired to a Lakeshore 340 PID temperature controller. As the current through the heater was adjusted, the temperatures were recorded and the voltage drop across the heater was measured using a 4-wire method. The heater power dissipation thus represents the available cooling power at the temperature measured by the thermometer on the far side of the plate.

Table 6. Net 4 K cooling power measurements

| Heater Temperature (K)	Cold Plate Temperature (K)	Heater Current (mA)	Heater Voltage (V)	Net Cooling Power (W)
4.19	4.004	16.8	9.606	0.161
4.44	4.249	19.4	12.82	0.249
4.68	4.500	21.3	15.34	0.327
4.93	4.750	23.0	17.88	0.411
5.19	5.002	24.3	20.02	0.487
5.68	5.499	26.7	24.03	0.642
6.19	6.005	28.7	28.15	0.808
7.19	7.001	32.4	34.91	1.131
8.20	8.000	35.6	41.62	1.482
9.21	9.001	38.4	48.24	1.852
10.2	10.000	40.5	53.22	2.155

From the data in Table 6, we can conclude that of the total 1.5 W cooling power at 4.2 K, 1.25 W of cooling power is used to mitigate the parasitic heating effects of radiation from the shields and heat transport through the wires.

The net cooling power of the system is lower than predicted. A major contributor to this result is insufficient heat conduction through the flexible copper braids connecting the pulse tube and the cold stages. A design for a flexible braid with a much larger total cross-sectional area is underway.

3   Laser Interferometer Metrology System

Testing of precision interferometer scanning mechanisms at 4 K requires optical metrology. Linear encoders that operate at 4 K are available, but suffer from relatively low accuracy, calibration issues, and parasitic thermal loading. In order to test and calibrate the metrology systems of prototype interferometer delay lines, a differential laser interferometer that can be mounted outside the cryostat was purchased using external funds.

The Renishaw RLD10 DI high resolution differential interferometer provides position feedback of the relative displacement between two plane mirror targets. This method of metrology ensures accurate positioning of critical components and eliminates common mode errors. The optics involved are completely enclosed in the Renishaw detector head which can be mounted on the outside of a vacuum chamber. Measurement beams have individual pitch and yaw adjustors can be modified at the detector head, eliminating the need to enter the vacuum chamber to make alignment adjustments. Using the RPI20 parallel interface, position measurements can be taken with a 38.6 pm resolution.
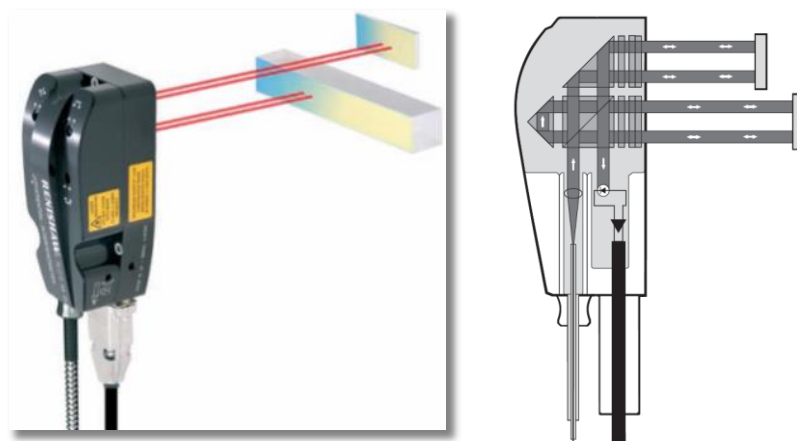
Figure 15. Renishaw Differential Laser Interferometer uses two pairs of optical laser beams to measure the relative displacement between two plane mirror targets. A quadrature signal is produced, indicating relative displacement magnitude and direction.

3.1   Initial testing of the differential interferometer

The differential interferometer was initially used for measuring the temperature-dependent thermal contraction of materials intended for use in the large test facility cryostat construction. Due to the long cool down times involved, and the fact that the differential interferometer only measures relative motion, the interferometer output had to be recorded continuously for durations of ~5 hours, but the software provided with the interferometer only provides a 20 second maximum recording time. To provide sufficiently long time series measurements, a custom electronics readout system was designed and built. A USB-based microcontroller (Teensy++2.0 [13]) was employed to interface the Renishaw RPI20 card with a PC. The card accepts analogue 1 Vpp sine/cosine signals, converting them into a 36-bit word and recording positional data at the 38.6 pm resolution. The microcontroller reads the Renishaw's 36-bit position

encoder output with an external digital clock trigger since the microcontroller is not capable of real-time time stamping. Overflow conditions were included in the microcontroller code since missing a single sample would corrupt the time series. Data collection was started and stopped using manual switches, since polling the serial port for commands drastically slowed the collection rate. The maximum continuous reading frequency before the overflow condition was triggered was ~17 kHz. For this application, 5 Hz sampling over a period of several hours was sufficient and produced manageable file sizes.

Table 7. Renishaw Differential Interferometer detector head specifications.

Beam Diameter	3 mm
Beam Separation	7 mm×14 mm
Alignment tolerance	±25 arcseconds (1m axis)
Beam alignment adjustment	±1° pitch
	±1° yaw
Maximum range	1 m
Sample rate	~17 kHz
Resolution	38.6 pm

The laser interferometer system was coupled to the translation stage of one of our laboratory FTS in order to verify its operation, as shown in Figure 16. The resolution of the raw interferometer quadrature signal was confirmed to be 158 nm by comparing against a Heidenhain glass encoder with 4 µm pitch [14].
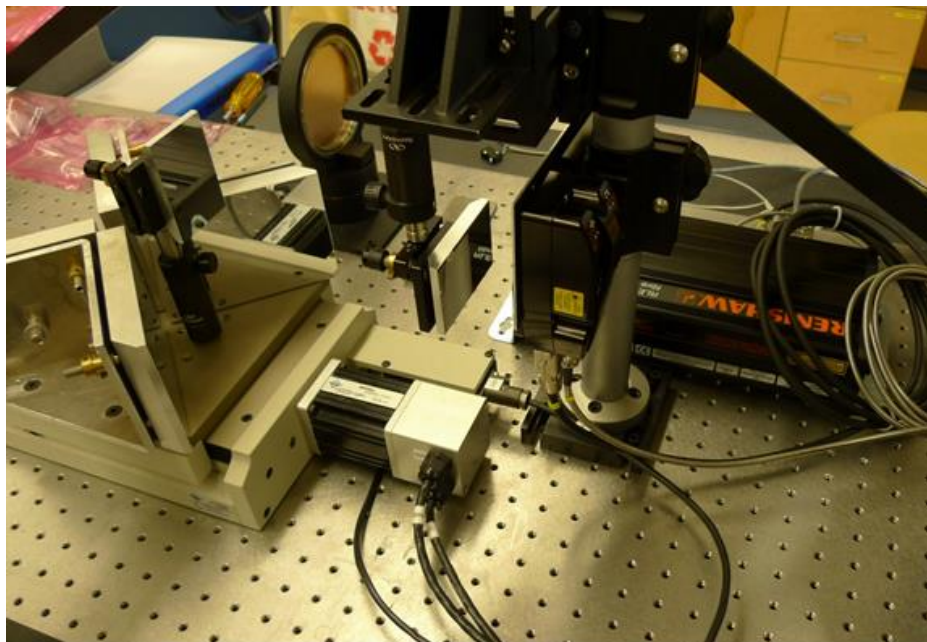
Figure 16. Testing the laser interferometer against a Heidenhain linear encoder. The interferometer head is shown at the centre mounted to the vertical post. The stationary reference mirror can be seen to the left of the head; the moving mirror is mounted at the apex of the FTS moving mirror assembly at the left.
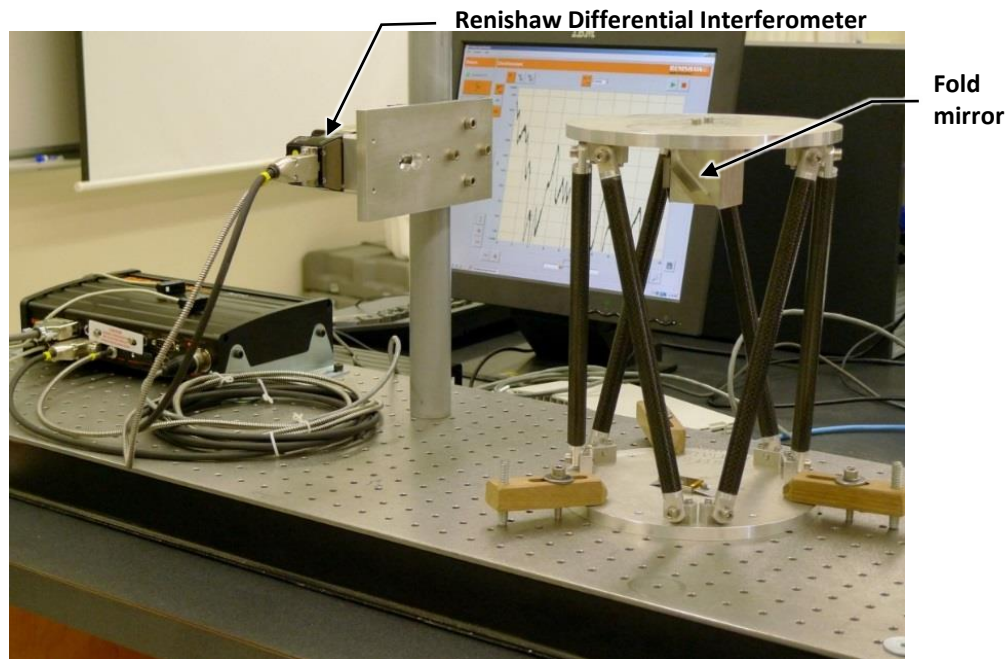
Figure 17. Oscilloscope trace of the Renishaw interferometer Sine quadrature signal (top) and the FTS Heidenhain optical encoder quadrature signal (bottom) as the FTS mirror is scanned at a constant velocity of ~1 mm/s. The interferometer resolution is 158 nm whereas that of the Heidenhain is 4000 nm.

The initial setup for measuring temperature-dependent thermal contraction began as a system of struts arranged as a hexapod with aluminum end plates, in order to mimic the hexapod configuration of the planned cryostat framework design. In order to simplify the measurements and make best use of the available space, the hexapod was required to be aligned along the cylindrical axis of the cryostat, but the original 4 K cryostat was constructed with optical feedthroughs only on the side walls of the vacuum chamber. A fold mirror was added to the hexapod structure in order to direct the Renishaw measurement beam along the axis of the hexapod. Plane mirror targets were placed beside the fold mirror for the reference beam and on the bottom plate of the hexapod for the measurement beam. The setup for testing the concept of this fold mirror design is shown in Figure 18. A load of 228 N was applied to the platform, resulting in a 44 μm difference in the optical path length. When the load was removed, the hexapod returned to the original length with no significant hysteresis. This compression was larger than expected for the typical Young's Modulus of CFRP, due to the effect of the bolted joints, but the measurement served as a proof-of-concept for the cryogenic tests.

Figure 18. Testing the hexapod design concept on the bench. The diagonal fold mirror is shown hanging off the top plate of the hexapod.

3.2   Measurement accuracy in cryogenic applications

In order to get an accurate measurement of the vertical contraction of the CFRP hexapod and tripod structures discussed in section 4.1, the reference and measurement laser beams must be exactly perpendicular to the mirrors on the surfaces under test and the mirrors must remain parallel. During the initial cool down, it was noted that the retro-reflected laser beams quickly diverged as the hexapod contracted, most likely due to a misalignment of the plates/mirrors. The sensitivity of the interferometer to motion perpendicular to the measurement beam was investigated by placing the interferometer on an x-y translation stage and tracking the beams across the surface of the mirror block while measuring the difference in optical path (Figure 19). The measurement error for parallel and perpendicular translation with respect to the beam is shown in Figure 20.
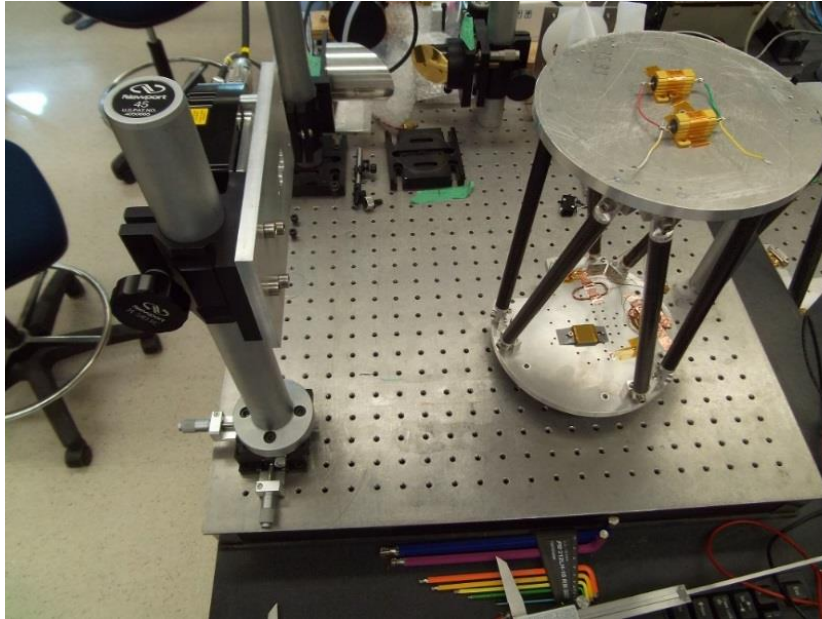
Figure 19. Testing the effect of misalignment of the mirrors in the hexapod system by scanning the laser interferometer head on an x-y translation stage.
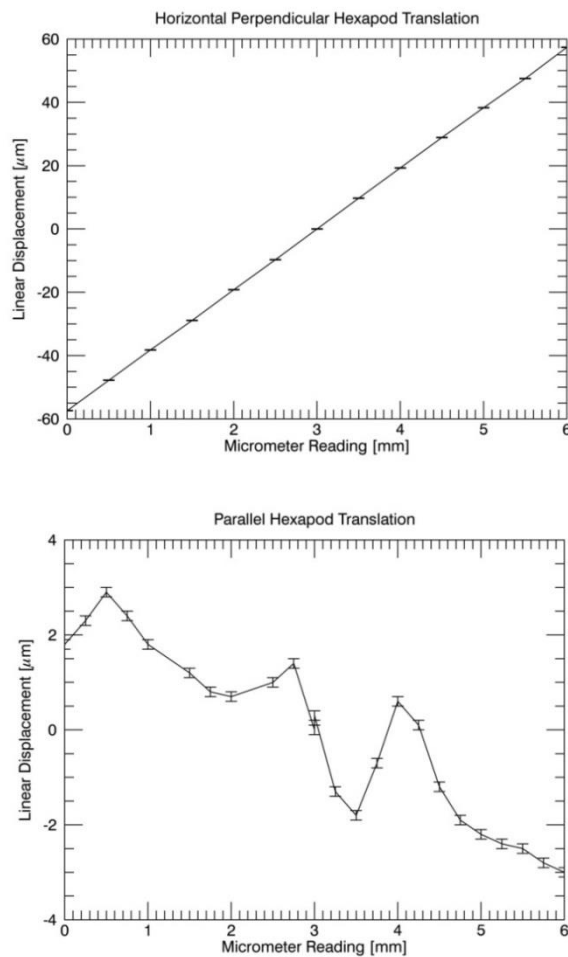

Figure 20. Measurement error due to motion of the interferometer head perpendicular to the beams (top) and parallel to the beams (bottom). The differential measurement effectively cancels parallel motion, but is sensitive to drift of the beams across the tilted mirrors.

In addition to alignment errors due to the tilted mirrors, vibrations from the pulse tube were clearly evident in the interferometer measurements. Some vibration was expected, but the amplitude was large enough to make contraction measurements difficult, and indicate that the folded optics are not suitable. Figure 21 shows the effect these vibrations have on the measurement when the cool down cycle is initiated.
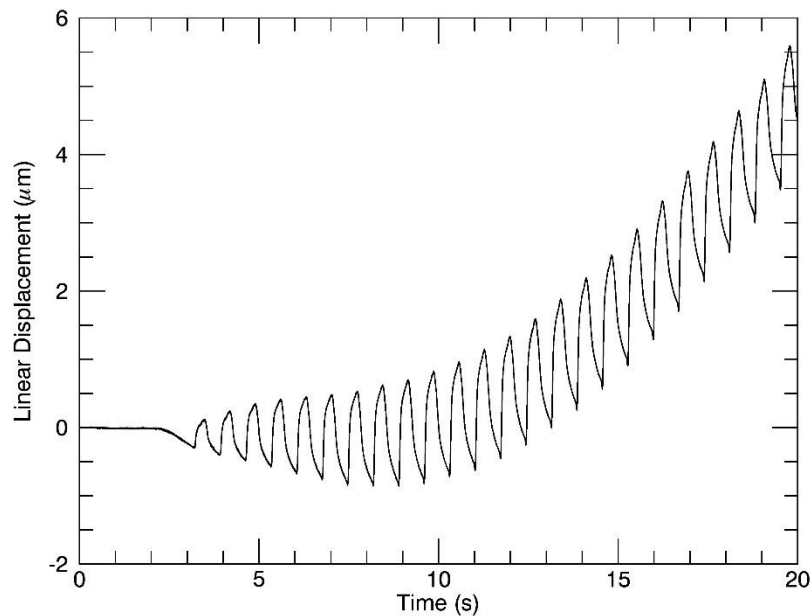
Figure 21. Measured displacement in the hexapod structure as the pulse tube cooler is turned on. The ~1 Hz oscillations are due to pressure waves in the pulse tube; the slow drift is due to contraction of the hexapod and cryostat structures.

As with any pulse tube cooled system, vibration caused by pressure changes in the pulse tube must be controlled when performing sensitive measurements. Vibration isolation mechanisms are normally employed, but were not included in the small test cryostat due to time and budget constraints. In this case, however, the largest vibrations component is along the axis of the measurement and the differential interferometer should be largely insensitive to these common-mode displacements. The only vibration effects that were evident were traced to imprecision in the alignment of the 45° mirror block. The operating frequency of the pulse tube is 1.3 Hz, resulting in vibrations at that frequency and its harmonics. Additionally, large compressors and vacuum pumps running in the laboratory contributed to vibrations of ~60 Hz and their harmonics. Figure 22 shows the frequency spectra of the interferometer position measurement when the pulse tube is running and turned off.
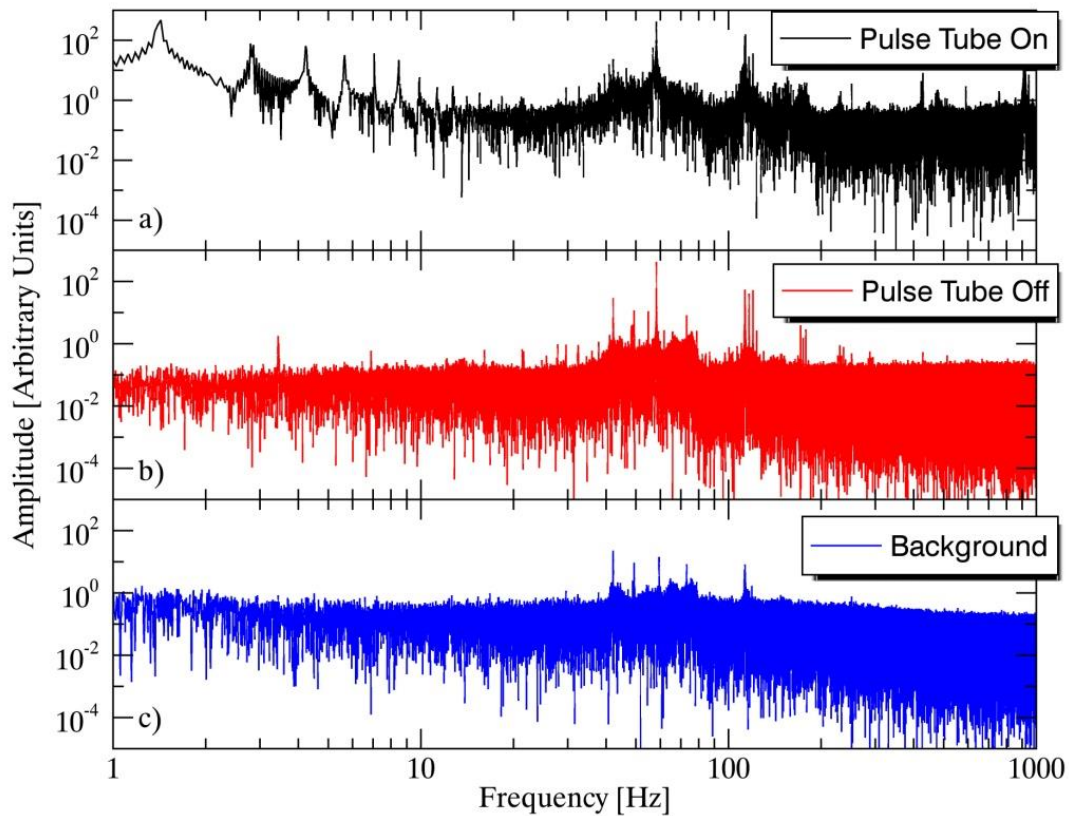
Figure 22. Power spectrum of displacement noise measured with the Renishaw DI: a) Normal operation; b) Pulse tube off, turbo vacuum pump on; c) Background noise (cooler and pump off).

With the hexapod arrangement, the vibration noise limits the instantaneous displacement measurement resolution to ~1 um, as seen in Figure 23. By changing the design of the structure to a tripod arrangement of vertical CFRP struts and by making small adjustments to the tilt of the two aluminum plates in order to ensure contraction only along a single axis, the overall measurement resolution during pulse tube operation was improved by an order of magnitude. As shown in Figure 22, the absence of the vibrations induced by the pulse tube could allow for at least an order of magnitude improvement in the measurement noise floor. Isolation from large compressors and vacuum pumps around the lab could allow for a further improvement. Since the pulse tube vibrations are induced primarily only along the axis of contraction an axial-viewing window was mounted in the bottom of the cryostat which allowed measurements to be made without the 45 degree mirror, which had been shown to induce errors. In this configuration the RMS measurement noise is expected to be of ~20 nm.
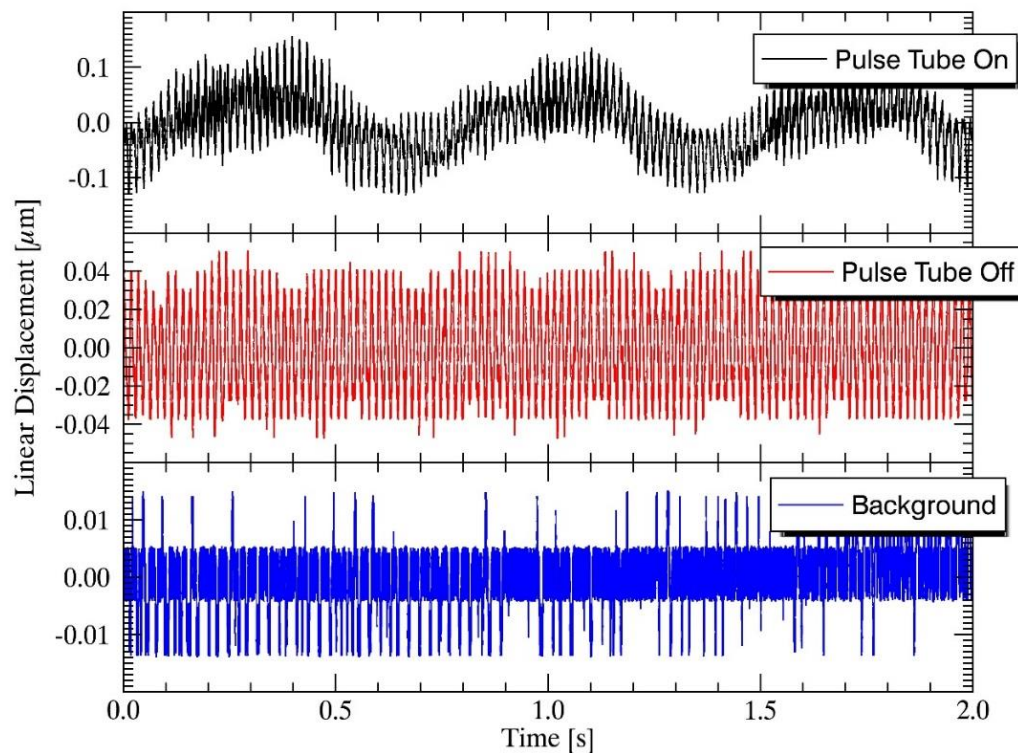
Figure 23. Noise measurement time series from the Renishaw DI: a) Normal operation; b) Pulse tube off, vacuum pump on; c) Background noise (everything off).

3.3 Suitability of Quartz viewports for interferometry at 4 K

A 50 mm diameter, 5 mm thick, uncoated fused silica window was added to the cryostat viewport for the interferometer measurements. Fused silica exhibits efficient transmission (>80%) in the wavelength range of 0.2-2.2 μm. With the window completely covered by the Renishaw interferometer head and sealed with a rubber gasket, the total power incident on 4 K components from room temperature blackbody radiation is on the order of 46 mW.

Due to the Fresnel reflection losses at the Quartz-air/vacuum interface, a ~20% drop in the interferometer signal strength was observed, but no change was seen in the sensitivity of the interferometer nor to the alignment of the beams when passing through the window, so antireflective coating to reduce Fresnel losses was deemed unnecessary. It was also noted that reflections off the window had no effect on the displacement measurements even when the window and the beams were completely orthogonal.

4 4 K Material Testing

The combination of large volume general-purpose 4 K cryostats and the laser interferometer system provide a valuable tool for testing components and materials of interest for future actively-cooled space missions. Many materials are poorly characterized at these temperatures, and testing of integrated systems is essential to determine the actual thermal conductivity at interfaces.

4.1 CFRP

Carbon fiber reinforced polymer (CFRP) is becoming a material of choice for cryogenic applications due to its high strength to weight ratio. CFRP has also proven to be an effective thermal insulator and can be manufactured to have near-zero thermal expansion, making it an ideal candidate for cryogenic mechanical structures and possibly for lightweight optics. The biggest drawback of composite materials, however, is that material properties are strongly dependent on the fabrication process, the relative densities of components and fiber orientations. The properties we are interested in for purposes of this assessment are thermal conductivity, thermal expansion and Young's modulus.

The original horizontal cryostat design (see Figure 10) employed commercially available CFRP tube to support the 77 K and 4 K structures [15]. Individual tube sections and a hexapod composed of CFRP struts were characterized to guide the cryostat design and as a proof of concept for the measurement system, as described in the following sections.

4.1.1 Single CFRP strut thermal conductivity

Thermal tests were performed to measure the heat conduction along a single CFRP strut with a thermal gradient of 4 K to 60 K. One end of a strut was bolted to the 4 K stage and Cernox RTD thermometers were attached to both ends. A resistor heater was attached to the free end of the strut. It was found that a constant heater output of 160 µW was required to maintain a temperature of 60 K at the warm end. This gave an average thermal conductivity, $\bar{\lambda}$, of 0.015 W/(m·K) by the equation below, where $\dot{q}_{cond}$ is the average conducted power, A is the cross-sectional area of the strut, L was the length and ΔT is the temperature difference between the ends of the strut:
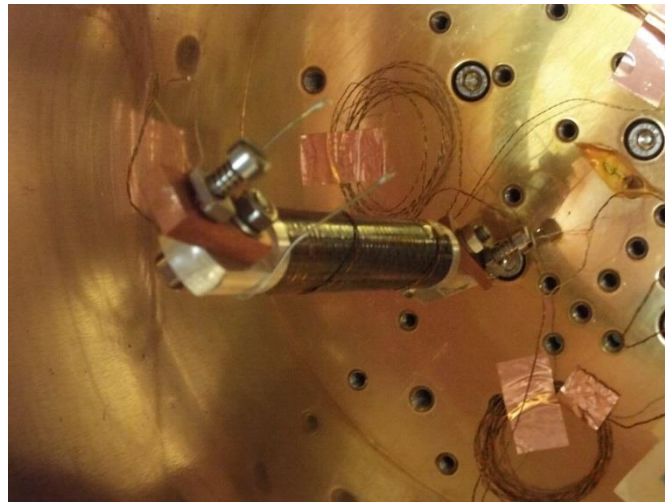
$$\dot{q}_{cond} = \frac{A}{L}\bar{\lambda}\Delta T$$

Figure 24. CFRP strut mounted on the 4 K for thermal conductivity measurements.

In order to improve accuracy, the thermal conductivity of this type of CFRP was measured over the entire temperature range from 4 to 300 K. In this experiment a short CFRP rod with aluminium end caps was bolted at one end to the 4 K stage. With thermometers on both ends of the rod, the temperature gradient across the rod was measured as the rod was cooled. The power flow through the rod was calculated for each successive measurement, using temperature information as well as the specific heat of the aluminium end cap and copper thermometer block attached to the free end of the strut, with corrections for radiative transfer and heat flow through the wires. The thermal conductivity at each average temperature of the rod is shown in Figure 25.
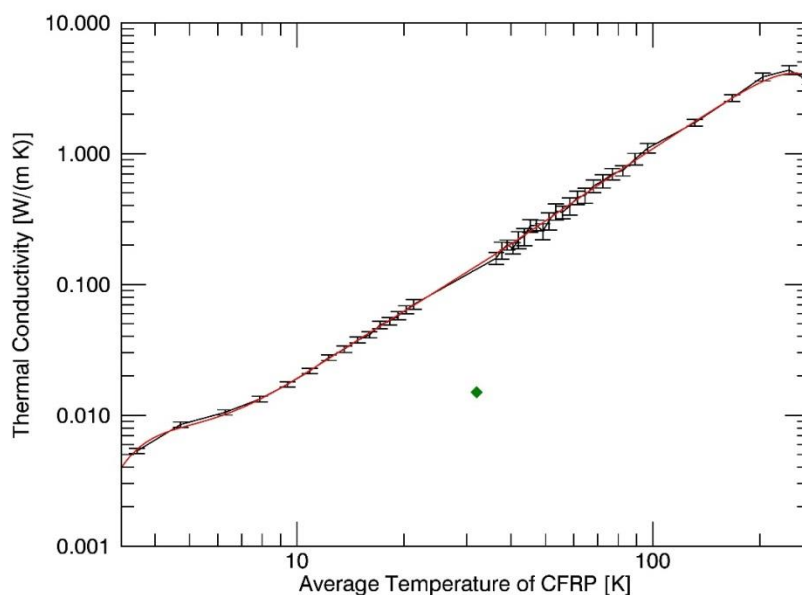
Figure 25 Measured thermal conductivity as a function of temperature for the CFRP strut, with measurement errors. The single green diamond indicates the single conductivity value determined in previous measurements. The red line indicates the polynomial fit to the data. The gap between 20 and 40 K was due to a computer malfunction during the cool down.

Temperature dependent thermal conductivity data was fit with an equation of the form:

$$\log_{10} k = a + b(\log_{10} T) + c(\log_{10} T)^2 + d(\log_{10} T)^3 + e(\log_{10} T)^4$$
$$+ f(\log_{10} T)^5 + g(\log_{10} T)^6 + h(\log_{10} T)^7 + i(\log_{10} T)^8$$

with units of W/(m·K) and the following coefficients:

Coefficient	Value
a	35.21
b	217.41
c	-604.08
d	923.51
e	-849.46
f	483.90
g	-167.37
h	32.24
i	-2.656

The functional form was chosen in order to easily correlate these measurements with standard databases of cryogenic material properties. This functional fitting form is used for all materials in NIST's cryogenic material properties database [16].

4.1.2 CFRP thermal conductivity and thermal expansion (Hexapod)

CFRP rods were assembled in a hexapod configuration in order to evaluate the mechanical properties of these struts when used as mechanical supports between the 300 K, 77 K and 4 K stages of a cryostat. Aluminium end pieces were glued to the CFRP rods with Torr Seal epoxy to allow the assembly to be bolted together [17]. Structural integrity of the epoxy joints was confirmed by multiple thermal cycles to 4 K.

The symmetry of the hexapod configuration results in net linear contraction of the whole assembly with insignificant tilting. In order to establish the coefficient of thermal expansion of the CFRP material, the contraction of the whole hexapod assembly was measured by placing mirrors on both end plates of the assembly and measuring the relative motion with a Renishaw differential laser interferometer. As noted in section 3.1, the limited volume of the 4 K cryostat dictated that the laser interferometer be mounted to a window, perpendicular to the direction of hexapod contraction. A 45° fold mirror was therefore required to direct the measurement beam to the fixed mirror on the bottom of the hexapod (see Figure 26).

Figure 26. The CFRP hexapod mounted inside the cryostat. A mirror block is attached on the underside of the upper plate with a vertical mirror for the reference beam of the interferometer and a tilted mirror that deflects the measurement beam to the mirror on the 4 K work surface.

### 4.1.3   CFRP thermal conductivity and thermal expansion (Tripod)

In order to make a more direct measurement of the strut contraction and minimize sensitivity to motion along other axes, the hexapod was replaced by a tripod of three CFRP struts oriented parallel to each other, as shown in Figure 27. The same test was repeated using the 45 degree fold mirror, and the cryostat was subsequently upgraded with an axial-viewing window on the bottom plate to allow direct measurement along the tripod axis.

Figure 27. The design concept of the CFRP tripod designed to replace the hexapod. This design allows for both folded and on-axis measurement with the laser interferometer, to directly determine the thermal contraction of the CFRP struts.

Using the 45 degree fold mirror, thermal contraction of the CFRP support struts was measured down to an average temperature of 70K. The insulating nature of CFRP prevented measurements at lower temperatures with this setup. Additionally, large thermal gradients caused warping of the struts which forced the Renishaw interferometer out of alignment. Further measurements with an axial view of the aluminum plates without the need for the 45 degree fold mirror will help rectify this current issue. Thermal expansion as a function of temperature was fit with a linear function of slope $1.95\pm0.01\times10^{-6}$ K^{-1}, which is the average coefficient of thermal expansion (CTE) for this temperature range for the CFRP struts. Published values of the CTE of CFRP composites encompass an extremely large range, -1×10^{-6} to 3.8×10^{-6} K^{-1}, depending largely on the direction of contraction relative to fiber orientation [18].
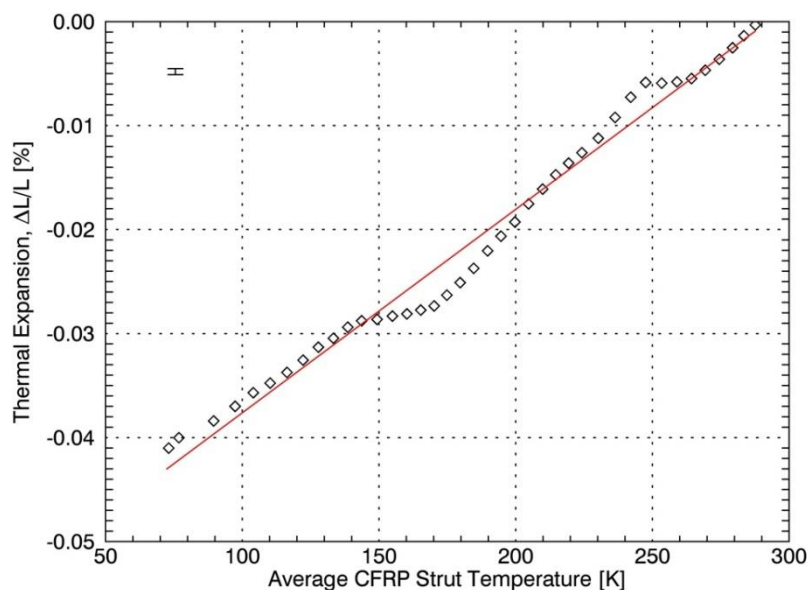
Figure 28. Temperature dependent thermal expansion of CFRP struts in the tripod assembly. Data points were fit with a 1st order polynomial to determine average CTE.

4.1.4 Design for CFRP sheet measurements

The measurement technique for evaluating the thermal contraction of CFRP described in the previous section is useful not only for a hollow rod arrangement but also for measuring the contraction properties of flat sheets of CFRP. In order to complete this measurement, we plan to modify the existing tripod arrangement by replacing the vertical struts with sheets of CFRP.

In collaboration with Martyn Jones and David Walker of Glyndwyr University, CFRP plates were constructed for use with an aluminium tripod configuration for measuring thermal expansion using the Renishaw Differential interferometer. Six sets of three plates each were constructed for thermal expansion measurement. These were comprised of two sets each of quasi-isotropic, 0° and 90° fibre orientation with respect to the tripod axis. The sample sets were labelled as indicated by the following table.

Fibre Orientation	Sample Label
Quasi-isotropic	Q-3-1, Q-3-2
90°	90-3-1, 90-3-2
0°	0-3-1, 0-3-2

The thermal expansion tests were conducted inside the newly fabricated TFC, making use of the vibration isolation provided by flexible copper heat straps in the facility. With the Renishaw mounted on a 50 mm viewport located on the short side of the vacuum chamber, the CFRP plate tripod was positioned horizontally inside the 4 K volume, facing the viewport. The 0° and 90° fibre oriented samples provided a means to measure the contribution of the fibres and epoxy respectively to the overall thermal contraction of a quasi-isotropic sample.
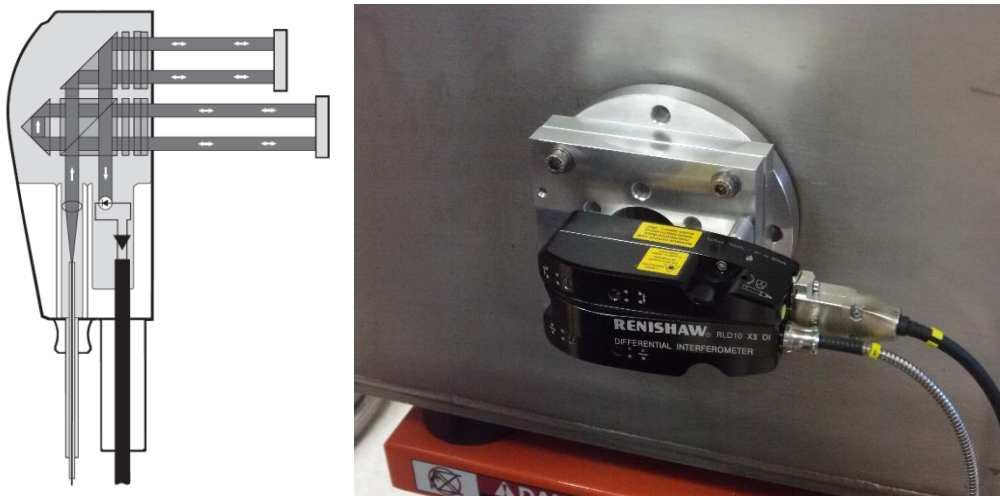
Figure 29. Schematic of the Renishaw Differential Interferometer and mounting plate for the TFC

Thermal expansion was measured with the Renishaw differential interferometer down to an average plate temperature of 50 K. The reduced vibrational noise induced in the test facility cryostat by the pulse tube cooler as compared to the older vessels was beneficial for ensuring the Renishaw stayed in alignment during the entire cooling process. The slower cool down time of the TFC also allowed for a smaller thermal gradient across the CFRP plates during the cool down. Base temperatures of the CFRP plate tripod were still higher than desired due to radiant loading from room temperature radiation entering though the cryostat window.
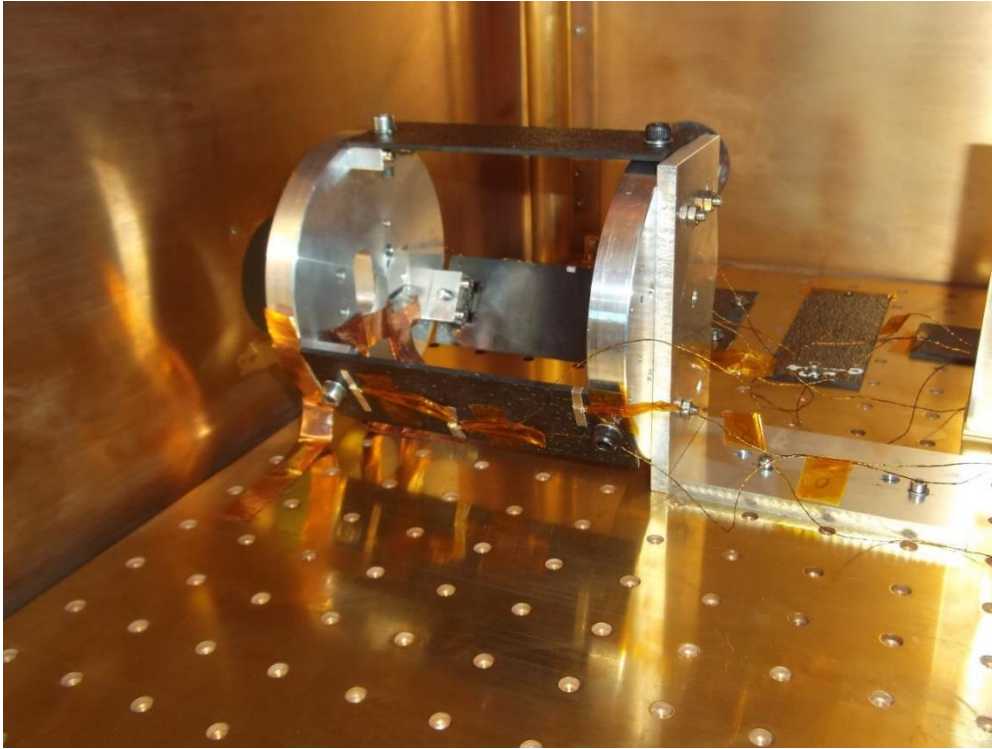
Figure 30. CFRP contraction measurement jig installed on the TFC 4 K plate. The beams from the Renishaw Differential Interferometer enter through the cryostat window on the left.
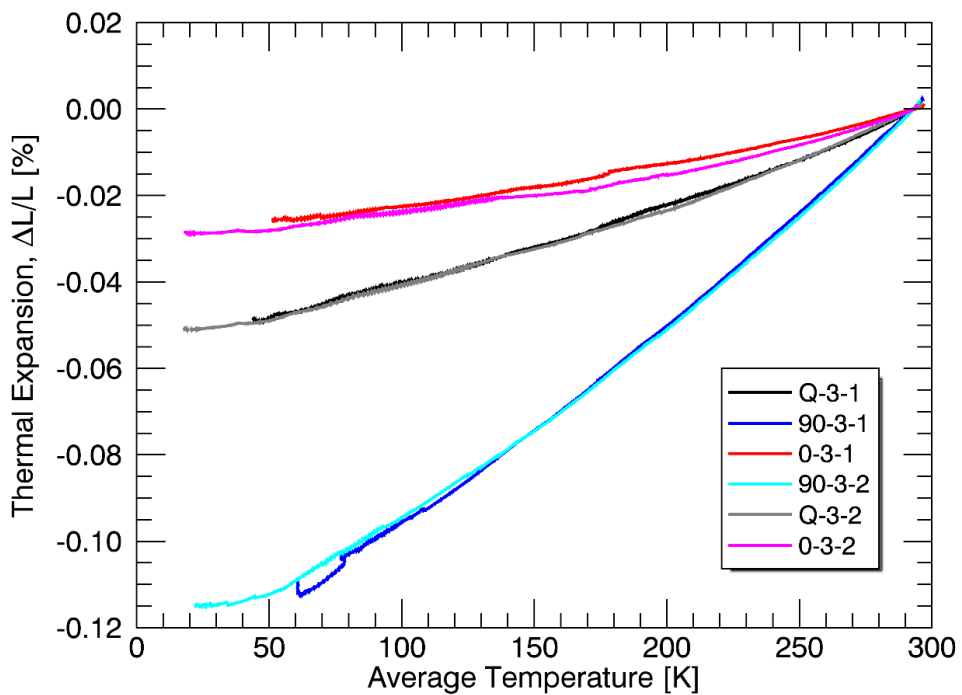

Figure 31. Thermal expansion of the Glyndwyr CFRP plate samples. The plates of each material type were cut from single sheets from the manufacturer.

In order to measure the effects of repeated thermal cycling on the physical properties of the CFRP samples, one set of quasi-isotropic samples was cooled to 20 K from ambient

three times. The data shown in Figure 32Figure 31 shows the change in thermal expansion, which we believe is due to fibre breakage at the microscopic level from thermal cycling and is currently being investigated [23].
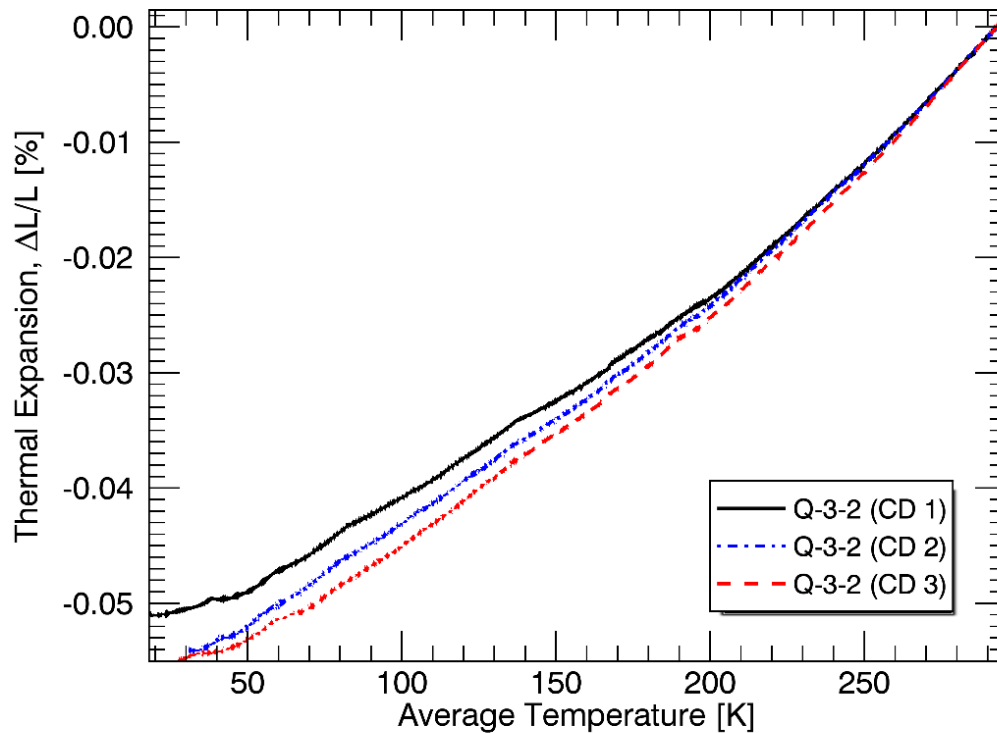
Figure 32. Variation in thermal expansion over three cooldown cycles for a single set of samples.

We are attempting to achieve lower minimum temperatures by reducing radiant loading. This will be accomplished with a cryogenically cooled iris which will be operated by a cryogenic Phytron stepper motor. The 4K iris will remain closed for the duration of the cool down to 4K, after which the stepper motor will open the iris so thermal expansion may be measured as the samples warm. We plan to continue measurements of CFRP thermal expansion with the second set of quasi-isotropic, 0°, and 90° samples.
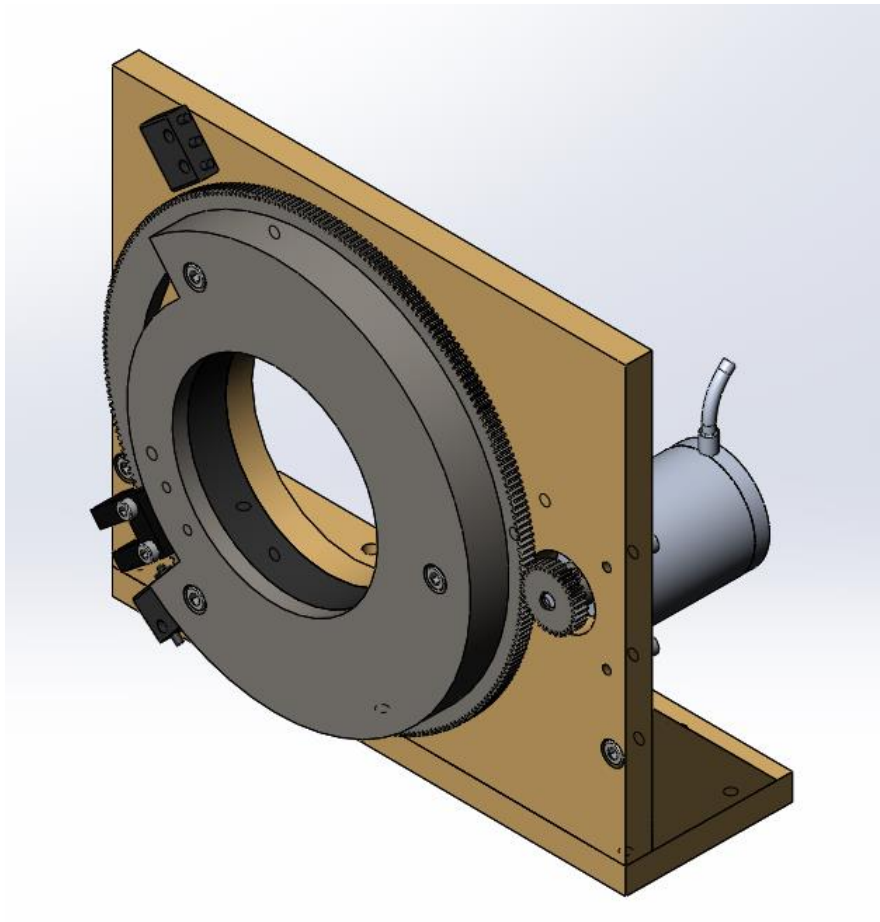
Figure 33. Design of the cryogenic iris.

We also plan to measure the elastic modulus of CFRP at cryogenic temperatures by adapting this apparatus to include a mechanical feedthrough in the cryostat to allow measured loads to be applied to the samples while the strain is measured using the laser interferometer. Based on an estimated value for the Young's modulus of CFRP of 1.3×10^{11} N/m^2 [22] and an expected measurement noise of 20 nm for on-axis dimensional changes, the minimum applied force would have to be ≥10 N for the existing samples. These tests may be done in the small 4 K cryostat, since it will be easier to modify the small chamber to accommodate the required mechanical feedthrough.

4.2   Copper residual resistance ratio (RRR)

Oxygen Free High conductivity (OFHC) annealed copper (typically grade C10100) can have significantly higher thermal conductivity below 4 K than standard grades of copper, but is much more expensive. In preparation for the manufacture of the 0.3 K detector mount and other components, samples of our current copper material supply were tested since an unknown fraction of it is OFHC. A standard technique to judge conductor purity is to measure this residual resistance ratio (RRR) which is defined as:

$$RRR = \frac{\rho_{295K}}{\rho_{4K}}$$

Where ρ_{295K} and ρ_{4K} are the electrical resistivities at room temperature and 4K respectively [11].

Strips of copper were cut to fit into the 4 K cryostat and wires were soldered onto the copper in a 4-wire resistance measurement configuration with a Lakeshore 370 AC Bridge. One end of each copper sample was held in contact with the 4 K stage to provide a good thermal link. The rest of the copper sample was isolated from the plate by a layer of Kapton tape [19]. A Cernox RTD was attached to the center of each copper sample to map its temperature[3]. The copper samples were cut in such a way that their room temperature resistances were approximately 1 mΩ and the lowest 4 K resistance was around 1 µΩ. We have determined that the measurement noise is low enough to determine which samples are regular grade copper and which are OFHC copper, but not low enough that an accurate RRR of each copper sample was achievable (see Table 8). This technique can also be used to verify the thermal conductivity of the critical sub-kelvin components in the 0.3 K detector system.
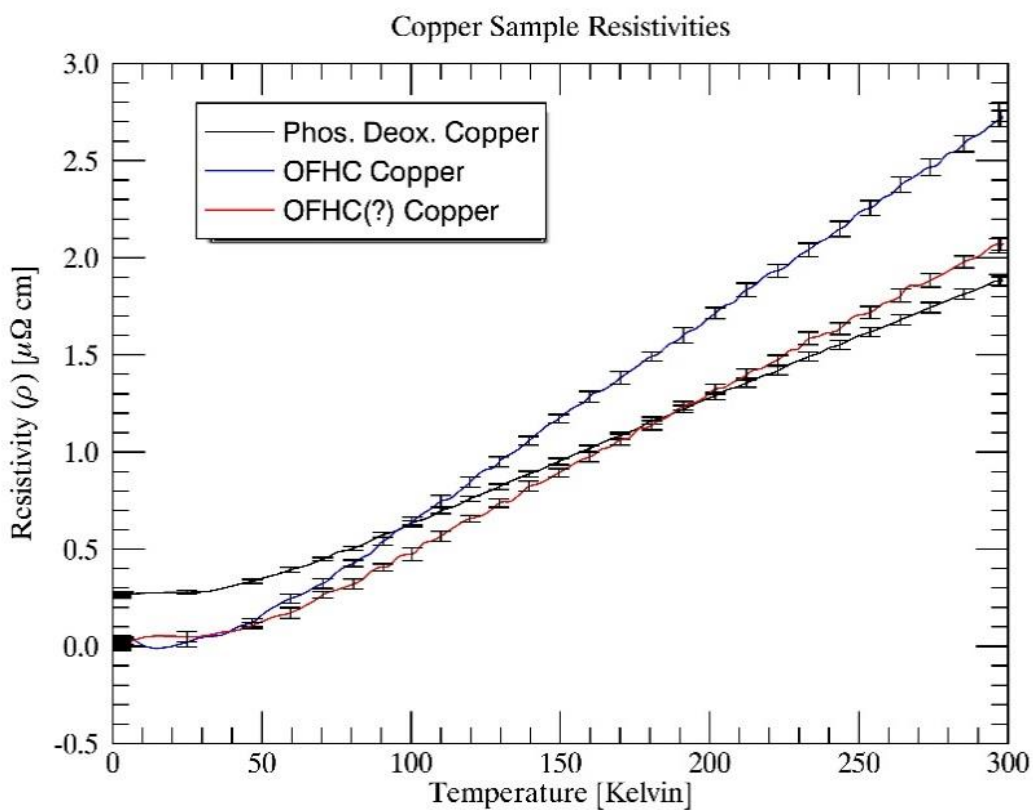

Figure 34. Measured resistivity as a function of temperature for various copper samples.

Table 8. RRR values deduced from experimental measurements shown in Figure 34.

Copper Variety	RRR
Phos. Deox. (C12200)	6.9±0.2
OFHC (C10100)	81±47
Unknown (OFHC?)	82±57

5   4 K Interferometer Delay Line

The large volume cryogenic test facility described in section 2 was designed to provide a suitable 4 K environment for testing interferometer delay line metrology techniques as well as for characterizing the thermal, mechanical and optical properties of materials at low temperatures. The initial plan was to procure the flight spare scanning mechanism of the Herschel/SPIRE instrument [20]. Unfortunately, the procurement process faced several logistical challenges and since there was only one flight spare it was decided that the risk was too great. Instead we have chosen to modify the scanning mechanism from a commercial laboratory FTS for operation at cryogenic temperatures. This will allow us to evaluate the performance of a differential laser interferometer mounted externally to the cryostat as a FTS metrology system and the integrated performance of the interferometer at cryogenic temperatures. With the large volume cryostat, we will be able to install a 0.3 K refrigerator with bolometer detector alongside the FTS, as well as a low temperature blackbody source, all contained within the low-background 4 K enclosure.

5.1   Bomem FTS design, modifications

The FTS scanning mechanism to be modified for cryogenic operation was removed from a defunct ABB Bomem IR spectrometer and is of the double pendulum design (Figure 35). This design was chosen because of its compact structure and voice-coil driven frictionless flex-pivot moving mechanism; both of which contribute to its suitability for use at cryogenic temperatures.

The ABB FTS operates by deflecting the wishbone arm with a voice coil. Rotating this arm moves one corner-cube retro-reflector away from the beam splitter and moves the other closer. This institutes a change in optical path length and results in the observed interferogram. In the typical laboratory configuration a HeNe laser beam running parallel to the infrared beam passes through the beam splitter off-axis, though apertures in the IR reflective beam splitter coating. A separate detector measures interference fringes from the monochromatic source to provide accurate optical path delay metrology. The optical path is shown in Figure 36. While this is an elegant design, the HeNe laser cannot be used within a cryogenic system. We proposed to use an internal a fiber launched laser metrology beam together with the external Renishaw differential laser to evaluate the performance of this FTS.

The FTS mechanism framework was trimmed to minimize the thermal mass and simplify mounting within the cryostat, as shown in Figure 37. The ZnSe beamsplitter will be replaced by a Mylar beamsplitter that allows the full 50 mm aperture to be used instead of the smaller sheared beams in the original design. Off-axis parabolic mirrors will couple the parallel interferometer beam to a small low-temperature blackbody source and f/3 feedhorn-coupled bolometer, as shown in Figure 38.

The voice coil actuator, flex pivot, and optical mounts must also be tested for operation at 4 K, as described in the following sections.
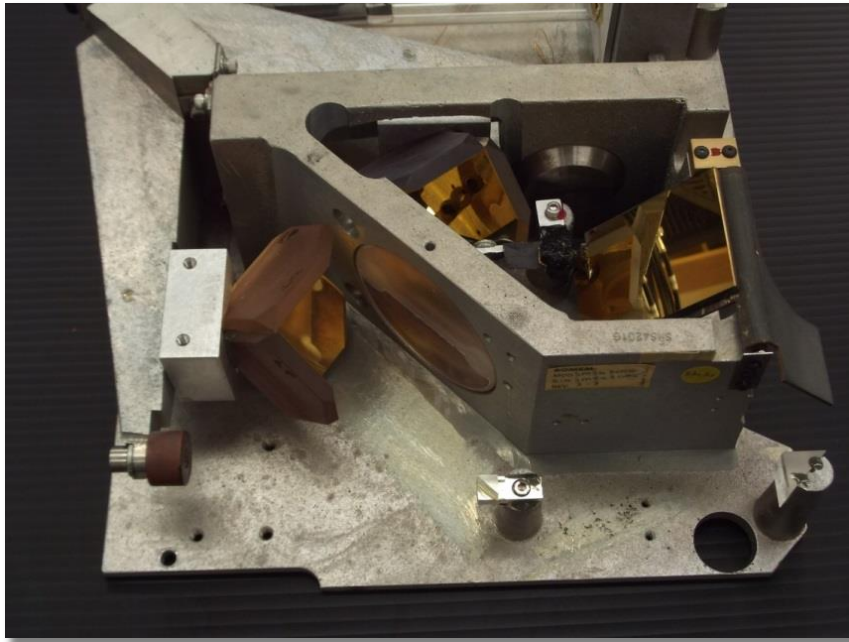
Figure 35. The ABB interferometer, with wishbone mechanism, original dual corner-cube retro-reflectors, and original IR beamsplitter.
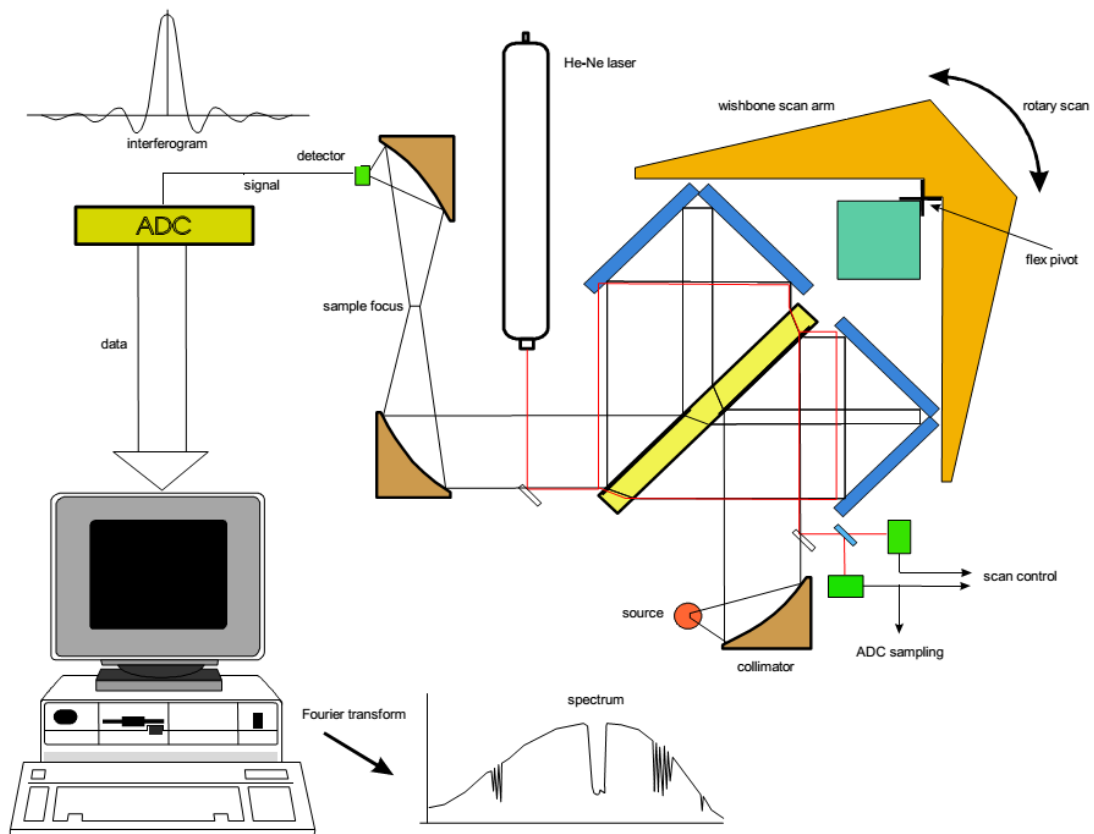

Figure 36. Schematic showing the ABB interferometer optics as well as the measurement and metrology beams.
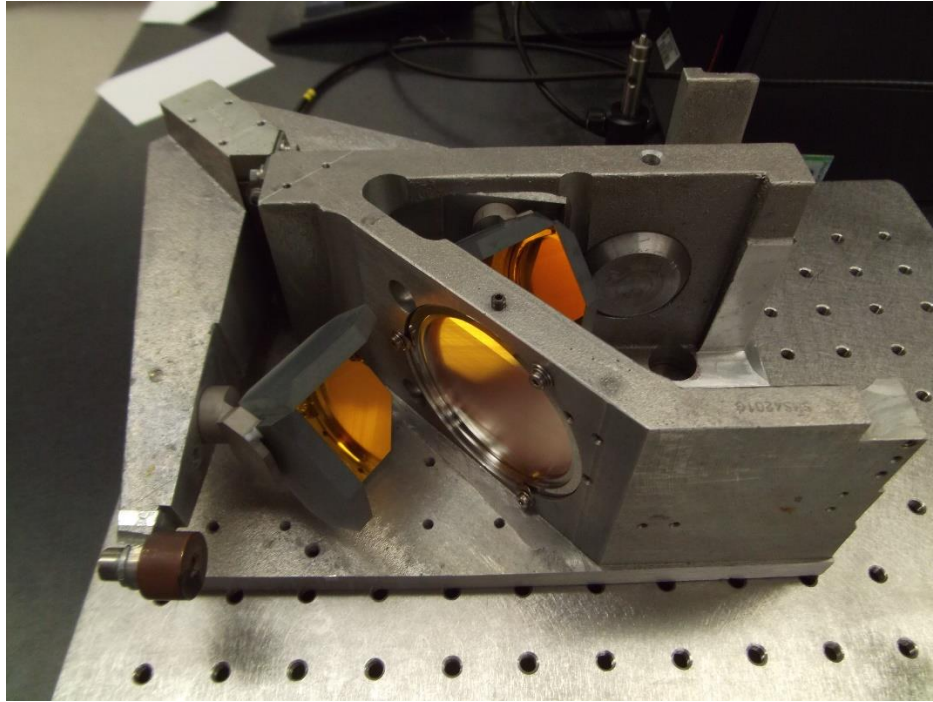
Figure 37. The ABB FTS mechanism retrofitted with thermally stable mirrors and far-IR beamsplitter.
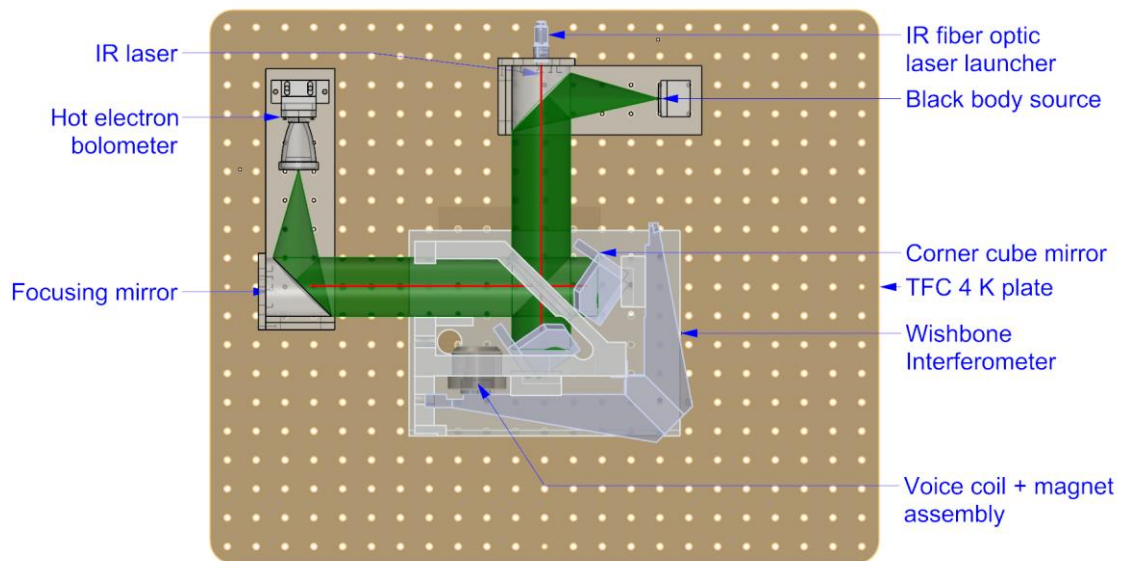

Figure 38. Schematic of the planned optical layout for the cryogenic Michelson FTS on the 4 K plate, including the ABB scan mechanism, two off-axis parabolic reflectors, low temperature blackbody source, 0.3 K detector and feedhorn.

5.2   Hall sensor magnetic sensitivity

In order to determine the temperature dependence of the magnetic field in the permanent magnet used in the voice coil for the ABB system, a Hall-Effect sensor was used to measure the field as the magnet was cooled. An InfineonHall Current Sensor was selected for use inside the cryostat, for its high sensitivity and linearity [21]. The integrated amplifiers in the chip, however, require an operating temperature of >130 K. A simple isolation platform and servo-controlled heater was constructed in order to keep the sensor at operating temperature (see Figure 39). The required operational temperature was determined by cooling the sensor and measuring its temperature

response to the magnetic field generated by the solenoid extracted from the ABB voice coil driver. The resulting magnetic sensitivity is shown in Figure 40. It was determined that the sensor has to be kept above ~130 K for optimal operation. This was easily achieved using a 1 kΩ resistor and a system of stainless steel bolts to isolate the sensor from 4 K.

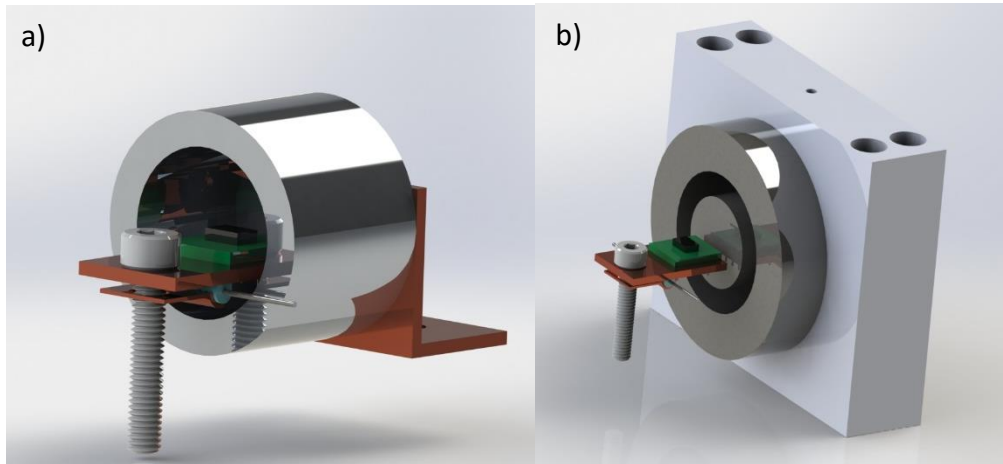**Figure 39. Setup for measuring the 4 K performance of Hall effect sensors within: a) the solenoid and b) the voice coil magnet.**
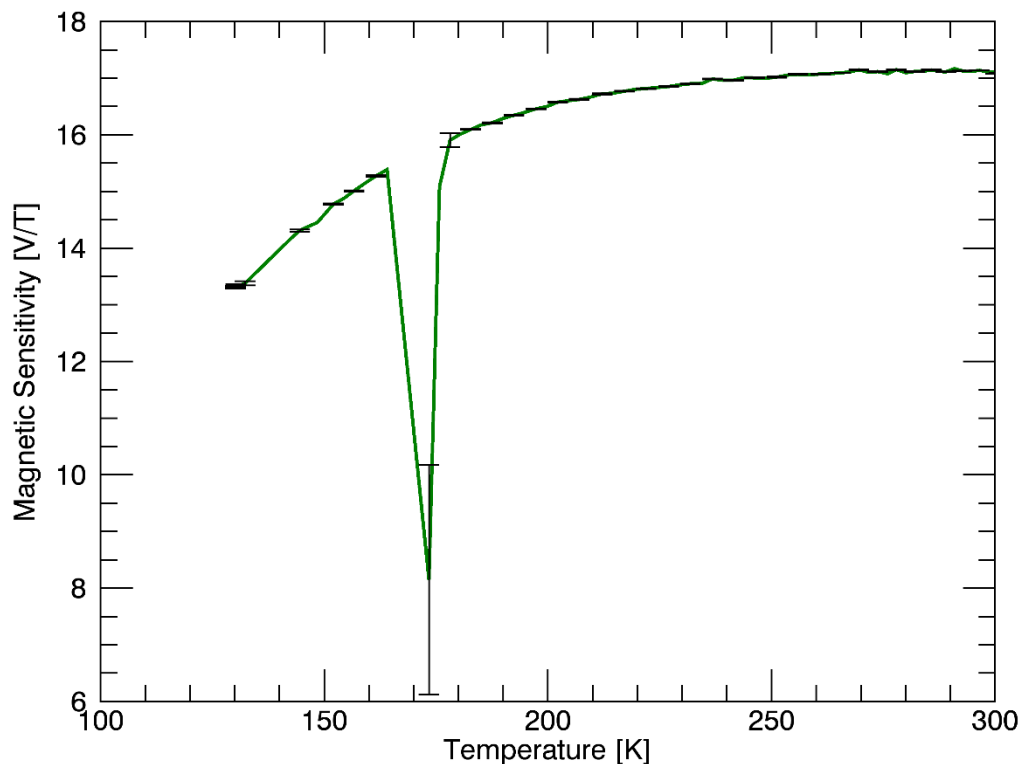

Figure 40. Temperature dependence and minimum operating temperature of the InfineonHall Current sensor with integrated amplifier electronics.

A wide range of Hall Effect sensors are available that are suitable for the required cryogenic voice coil measurements. The limiting factors are the power dissipation by the sensor and associated amplifiers, temperature calibration, and also the compactness of the sensor. The magnetic field of the permanent magnet in the voice coil was measured using a hall sensor that has been calibrated for 130 K operation and rated for magnetic fields of >50 mT.

5.3   Magnet specifications

The permanent magnet used by ABB is a HICOREX rare-earth cobalt magnet. These magnets are suitable for extreme temperature operation, exhibiting only small reversible changes in magnetic properties when exposed to low temperatures. Rare-earth cobalt magnets such as Samarium-cobalt, however, are known to be prone to fracture when subjected to thermal shock. To minimize thermal gradients during the cooling process, the magnet was press fit into an aluminum mount, allowing the magnet to cool in a radially symmetric fashion.

Figure 41 shows the percentage change in the magnetic field of the permanent magnet as it cools from room temperature. Here we show a relative increase in the magnetic field strength due to smaller thermal fluctuations in the magnetic dipole moment. Multiple thermal cycles to 4 K reveal that the change in field strength is reversible, with a small amount of hysteresis. From these results, we anticipated the voice coil would function at 4 K.
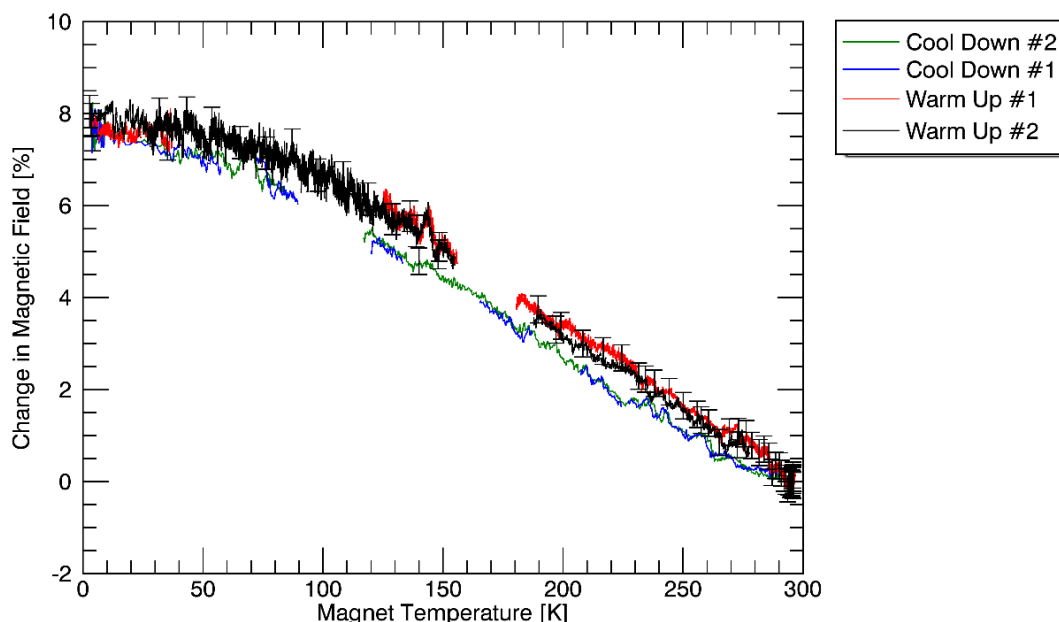

Figure 41. Percentage change in the magnetic field strength of the permanent magnet of the WBI voice coil. Measurements were taken over two complete thermal cycles of the magnet to 4K. Offset between the cool down and the warm up curves demonstrates a small amount of hysteresis upon thermal cycling. All magnetic field strength changes are reversible.

5.4   Beamsplitter design

The original ABB FTS IR beam splitter is made from ZnSe. Semi-reflective coatings are applied on the back side of the top half and front side of the bottom half with uncoated sections on the edges of the beam splitter for the measurement laser (Figure 35). The split design eliminates the need for a compensation plate, but requires a smaller (1") beam diameter. Unfortunately ZnSe does not transmit beyond 20 um. Prof Peter Ade will provided a broad band beam splitter similar to that used on Herschel/SPIRE interferometer for this purpose [20]. The new beam splitter has masked regions that will allow the laser metrology beam to sample the optical path of the interferometer, as shown in Figure 43.

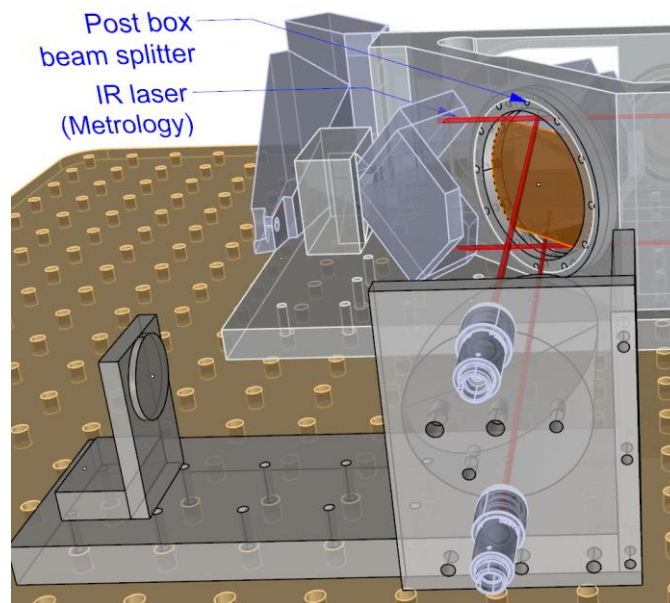**Figure 42. Post box beamsplitter.**

Figure 43. Sheared metrology beams in the interferometer, passing through the custom beamsplitter.

5.5   Corner Cube Retroflectors

The ABB FTS utilized two 2 ½" clear aperture, gold coated corner cube retroflectors. These corner cubes were held to the FTS arm with aluminum mounting blocks. Due to the large differential thermal contraction between aluminum and the glass mirror substrate, the corner cubes became detached from the frame after thermal cycling (Figure 44).
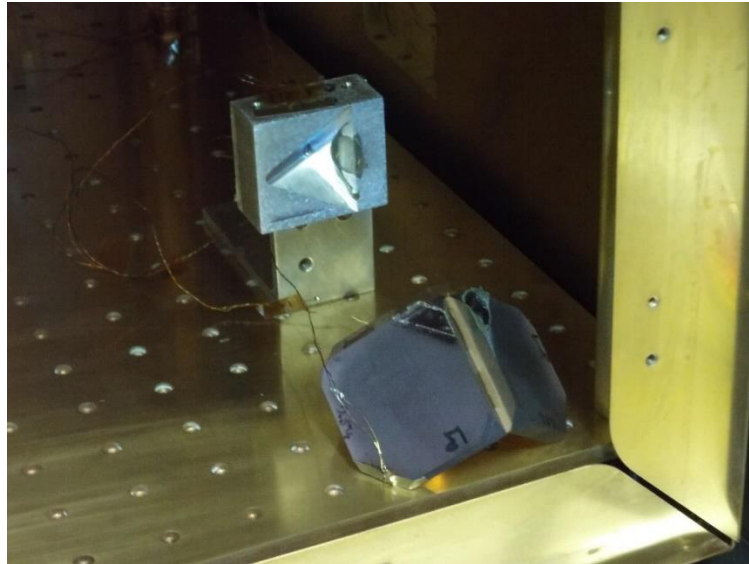
Figure 44. The original corner cube retroreflectors from the WBI after thermal cycling. The dislocation is due to the differential thermal expansion of the aluminum frame and the glass mirror.

As a solution to the thermal contraction issue, corner cube retroflectors were purchased with an Invar support frame (Figure 45). Through the process of thermal cycling and measuring the orthogonality of the mirrors with a PLX electronic autocollimator, we determined these corner cubes were suitable for both room temperature and cryogenic temperature operation.

Figure 45. Replacement corner cube retroreflectors with Invar frame. These corner cubes were tested at 4 K and maintained alignment both while cold and on return to room temperature.

5.6   Flexure Pivots

The interferometer moving mechanism consists of a rotating arm attached to the interferometer frame by thin, metal flexure bearings. The arm is driven by a voice coil. The original flexure bearing is fabricated from a 250 um plate of spring steel. The mechanical properties of the steel at low temperatures is unknown because the specific alloy is unknown. Many steel alloys are known to become brittle and have reduced fracture toughness at low temperatures, due to their b.c.c crystal structure. Therefore, the flexure bearings were replaced with Inconel 718 springs. Inconel retains its ductility over the cryogenic temperature range and has a space heritage, being used in flexure bearings for the cryogenic HIFI instrument on the Herschel Space Observatory. In addition, thinner bearings were considered in order to minimize the force requirements of the voice coil, minimizing the heat dissipation.

The thermal map of the ABB Bomem IR interferometer skeletal frame along with its wishbone arm was measured in the Test Facility Cryostat. The tests were performed while connected the wishbone arm to the frame using three different flexure leaf springs:

1. Stainless steel – thickness = 0.25 mm
2. Inconel – thickness = 0.13 mm
3. Inconel – thickness = 0.42 mm

A number of temperature sensors were placed at various locations on the wishbone arm and its frame to determine the cooling requirements of this interferometer when its arm is moved using different flexures.
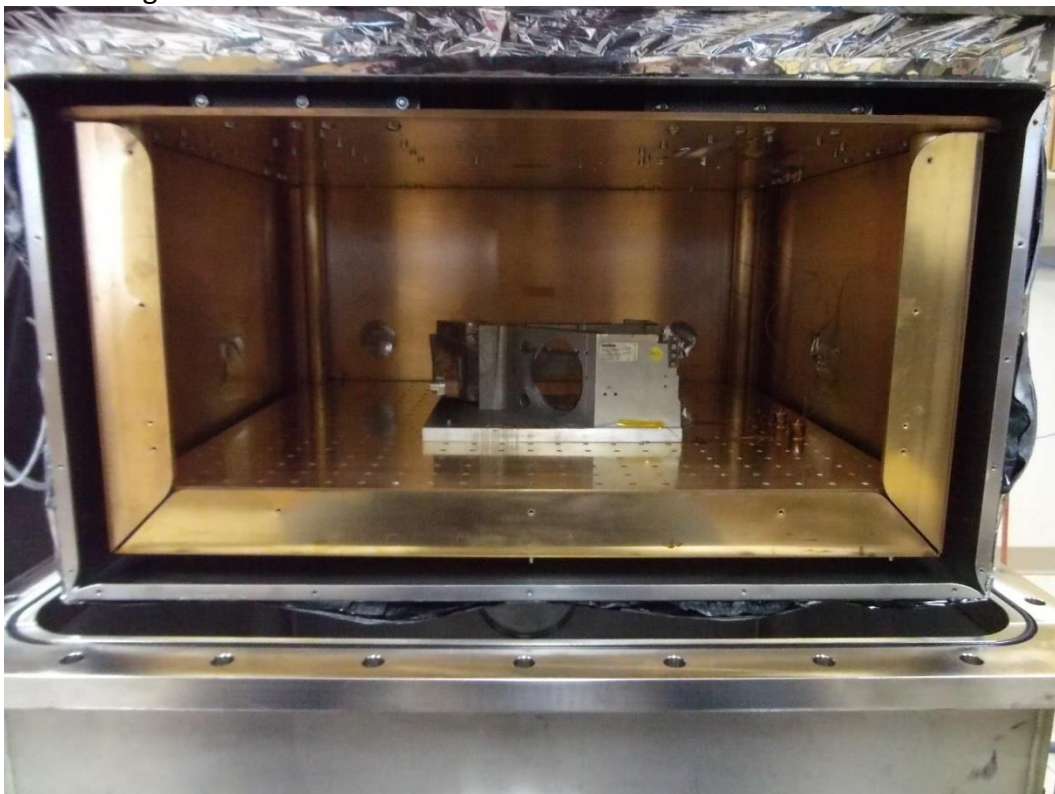

Figure 46. Wishbone interferometer chassis inside the TFC.

Error! Reference source not found. shows a typical thermal map and the related c ooldown curves when a wishbone arm is connected to its frame using a flexure leaf spring. The Test Facility Cryostat is precooled with liquid Nitrogen for 4 hours and the 4 K plate reaches its base temperature after 17 hours. The wishbone interferometer frame reaches 10 K about the same time that the 4 K plate reaches its base temperature, but it takes about 6-7 hours to reach the base temperature. The wishbone arm connected by the flexures requires another 10.5 hours. The temperature at different locations on each of the wishbone arm is within ~1 K, so the 5 sensors on the arm are all shown as the red curve.
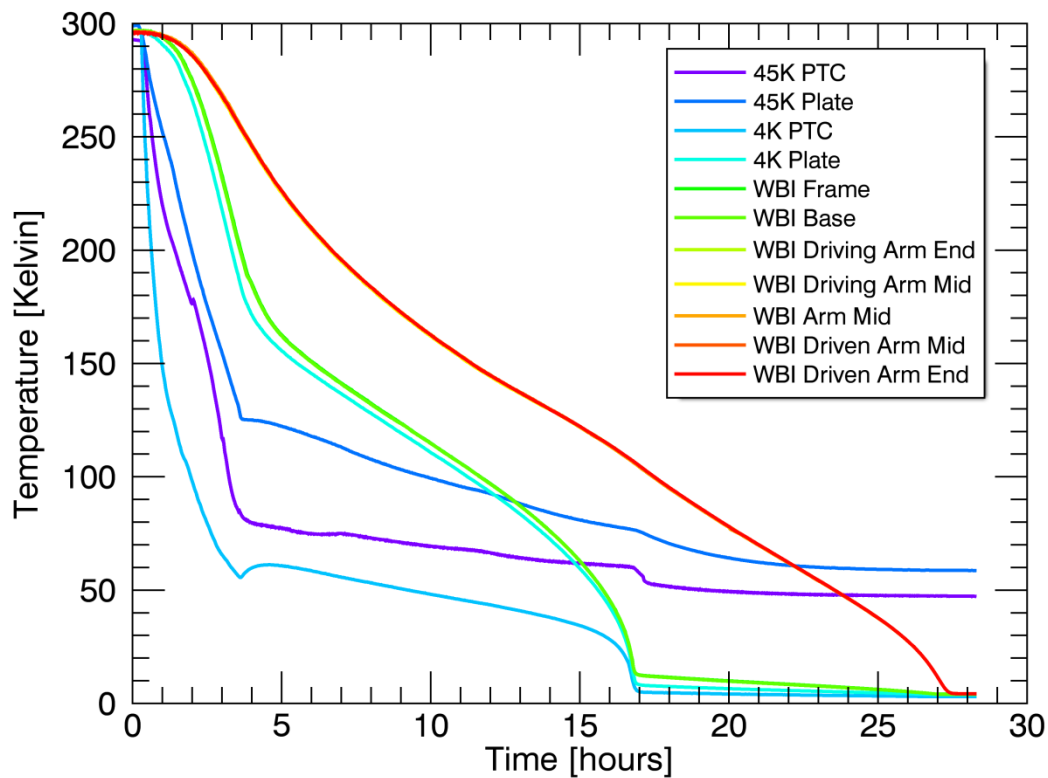

Figure 47 Thermal map of the wishbone interferometer

Table 9. Cooling times of the 4K plate and wishbone interferometer components with different flexure pivots.

	Cooling Time (hrs)		
Flexure type	**4K plate**	**WBI Frame**	**WBI arm**
Stainless steel	20.5	20.5 + 3.5	20.5 + 3.5 +0.6
Inconel 5	18	18 +27	18 + 27 + 5.5
Inconel 15	17	17 + 6	17 + 6 + 4.5

The reason for the different times to achieve the base temperature of 4 K is because of the different liquid Nitrogen precool times.

The flexure bearing was the only heat path connecting the WBI arm to the cryogenic surfaces. Therefore, changing the bearing to a thinner material significantly increased the cooling time, shown in Figure 48. Also shown in Figure 48, is the effect of including a 10 AWG, 10 mm long, OFHC copper braid between the WBI arm and frame across the pivot joint, pictured in Figure 49. Including the copper braid decreased cooling time of the arm by 20 hours, making the use of a 0.13 mm Inconel flexure bearing feasible.
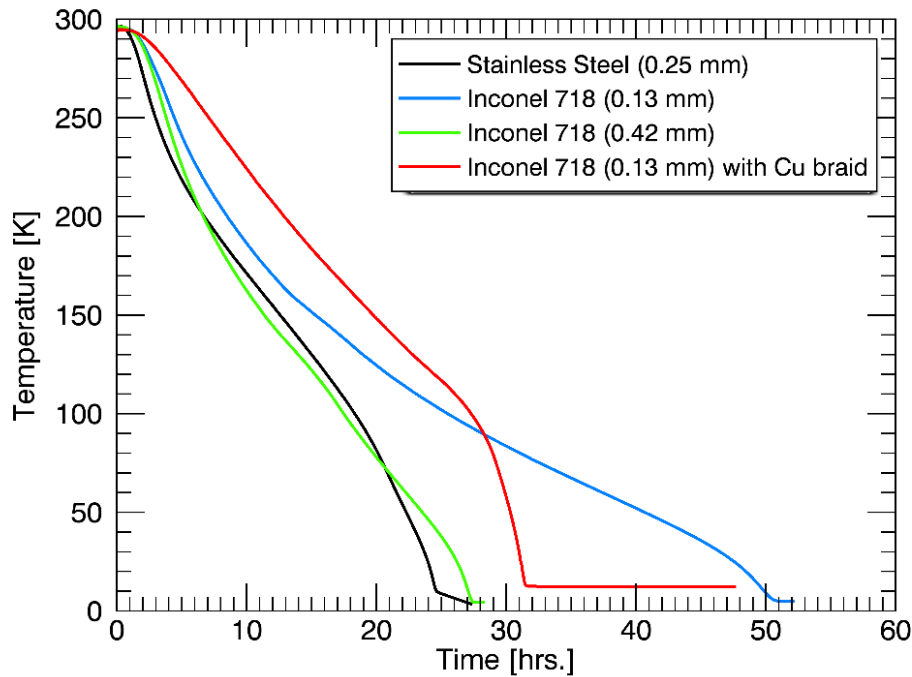

Figure 48. Temperature of the WBI arm during cooling. Nominal cooling time for the 4 K volume is 23 hours.

Figure 49. Flexible copper braid attached to pivot of the wishbone arm to aid cooling the arm.

5.7   Metrology

The metrology system is used to record interferogram samples in equal intervals of optical path difference of the wishbone interferometer. A 1.55 micron fiber launched laser based infrared metrology system was developed for use at cryogenic temperatures.

Figure 50 shows the IR laser launched using an optical fiber into the interferometer module. A plane mirror was mounted on the piezo-electric translation mechanism oscillating at a frequency of 10 Hz. The following figures shows the oscilloscope grabs of the metrology fringes at different time scales while the translation stage is motion.
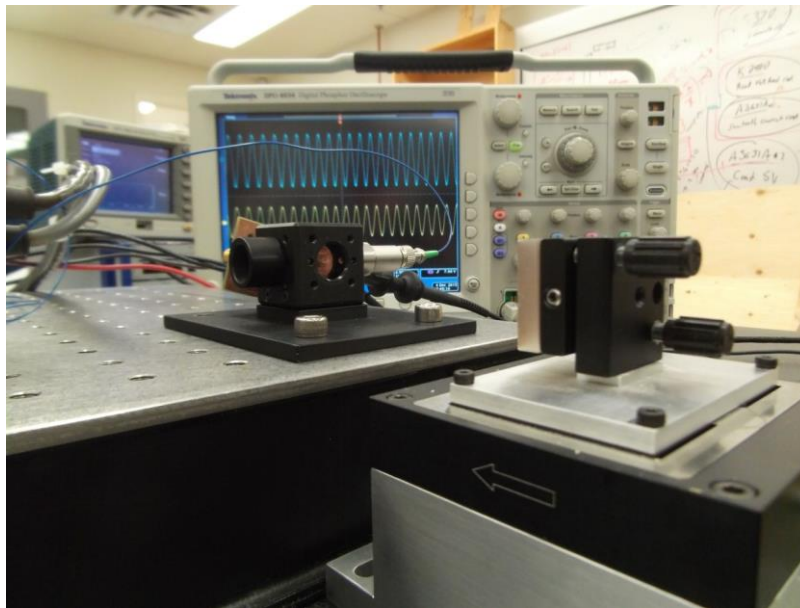

Figure 50. IR metrology system shown on an optical bench for testing. Fringes on the oscilloscope are the result of modulating the path difference by translating a reflecting mirror.
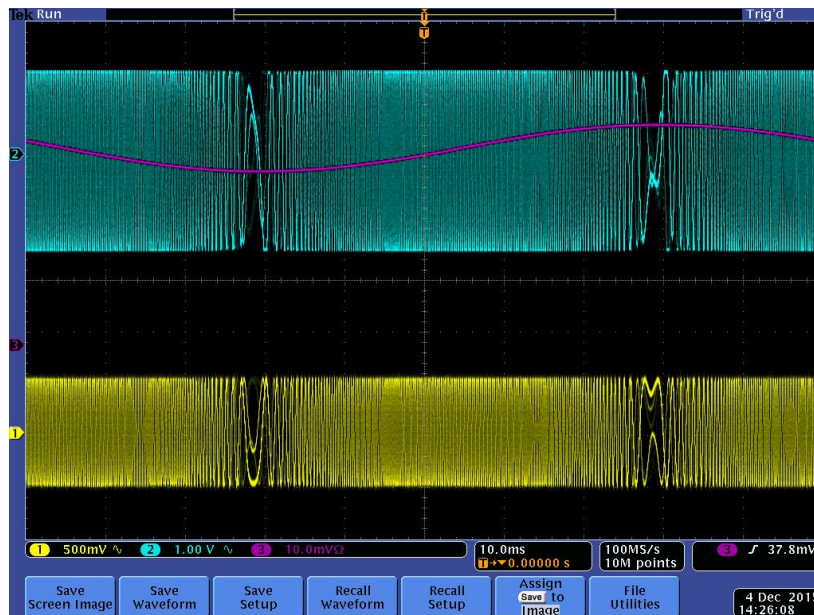

Figure 51. Oscilloscope readout of the frequency modulation in the IR metrology fringes due to the sinusoidal velocity of the mirror.
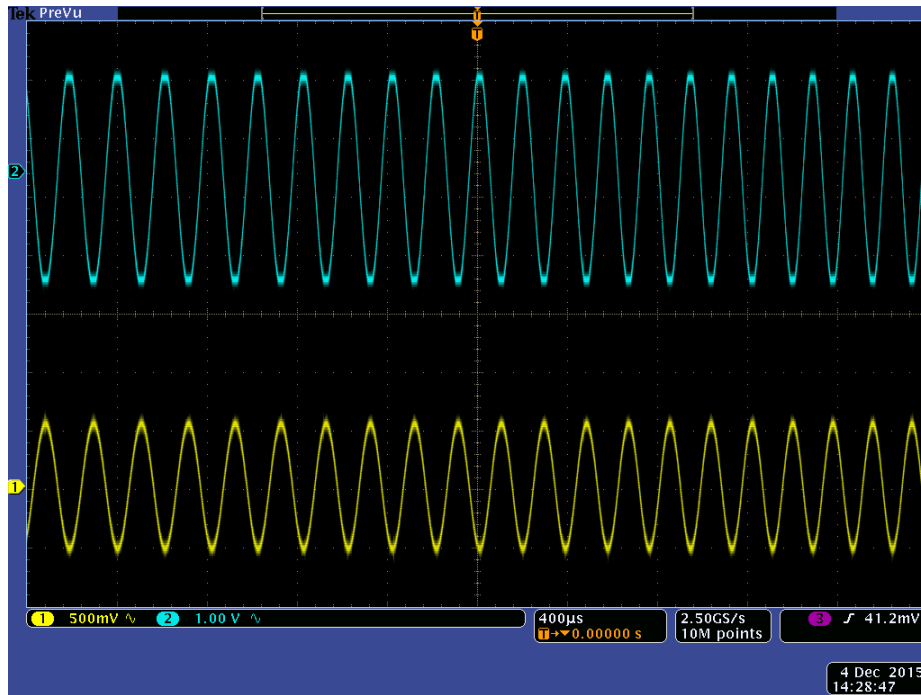
Figure 52. Oscilloscope readout of the IR metrology fringes while scanning the mirror at nearly constant velocity.

A Mylar beamsplitter is installed in the wishbone interferometer and the following fringes are observed on the oscilloscope using a HeNe laser. The wishbone arm is moved at a frequency of 2 Hz.
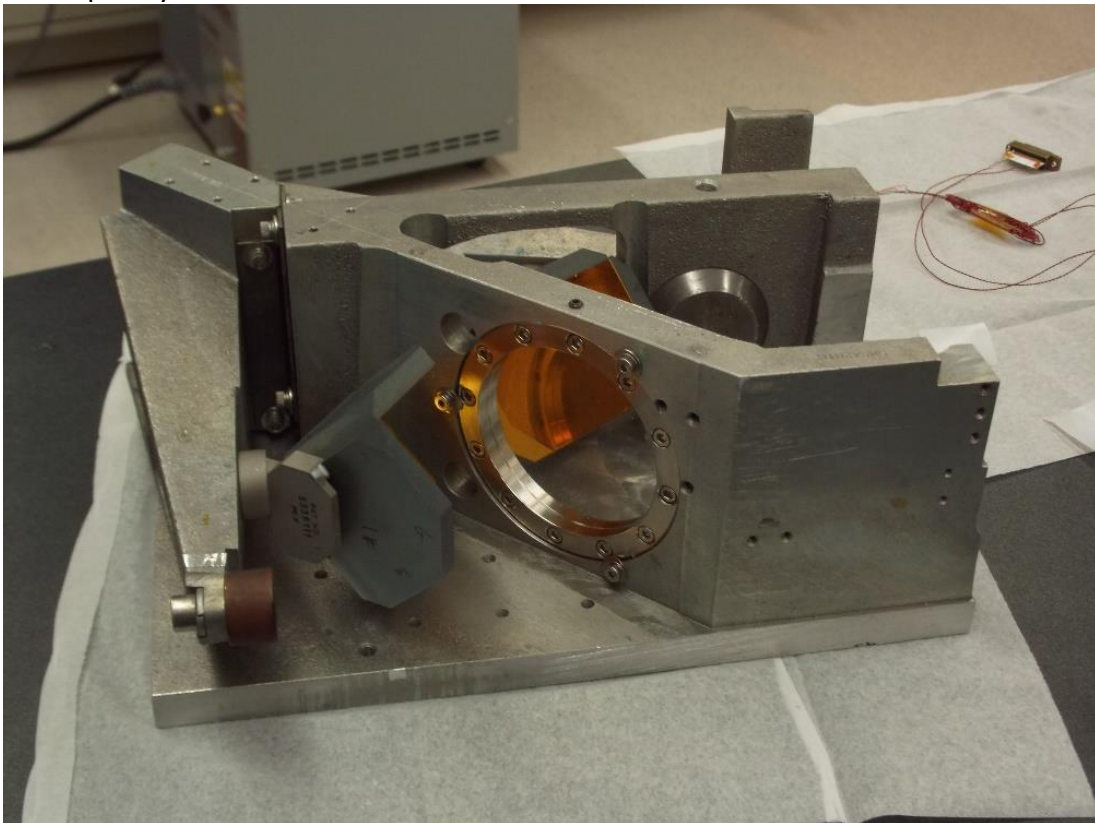

Figure 53. Image of the wishbone interferometer with a Mylar beamsplitter.

Figure 54. Interference fringes observed with a HeNe laser through the Mylar beamsplitter in the wishbone FTS. The scanning frequency of the FTS was 2 Hz.

Metrology has not yet been performed through the metal mesh, post-box beamsplitter because of excessive scattering of the metrology laser beam from the beamsplitter substrate.

5.8   Expected FTS performance

The development of the cryogenic FTS will continue. A number of challenges that are foreseen with the adaptation of this system for operation at cryogenic temperatures:

- Poor thermal conductivity across flexible joints leading to a lengthy cool down times.
- Thermal expansion causing undesirable stresses on fragile components. This includes the flexible pivots and the glue joints of the corner cube retro-reflectors. This may lead to the deformation of the corner cubes or loss of glue adhesion.
- Thermal induced deformation will require additional calibration of the FTS optical path difference metrology.
- Current requirements of the voice coil actuators will differ because of changes in the electrical resistivity of the solenoid as well as changes in the magnetic field strength of the permanent magnet.
- Beamsplitters will experience a change in reflection/transmission properties when exposed to cold temperatures.

The FTS will be initially operated in continuous scanning mode. Ultimately, a double voice coil driving system will be implemented to achieve step-and-integrate functionality for double interferometry tests. The following table lists the design specifications for the cryogenic FTS. The measured performance will be presented in deliverable D3.6.

Table 10. Expected specifications of the cryogenic FTS

Spectral Range	5-500 cm^{-1} with resonant mesh beamsplitter 500-5000 cm^{-1} with ZnSe
Spectral Resolution	<1 cm^{-1}
Beam Diameter	50 mm
Optical Scan Length	0.5 cm before and after ZPD
Scan Time	~1.s
Source	Internal low temperature blackbody
Focussing optics f/#	f/3, f/2
Mirror Diameter	50 mm

6 References

[1] S. P. Davis, et al., *Fourier Transform Spectrometry* (Academic Press, 2001).

[2] http://www.cryomech.com/products/cryorefrigerators/pulse-tube/pt415/.

[3] http://www.lakeshore.com/products/cryogenic-temperature-sensors/cernox/models/pages/overview.aspx.

[4] http://www.cryomech.com/products/cryorefrigerators/pulse-tube/pt403/.

[5] http://www.chasecryogenics.com/.

[6] S. Chase, "Three-Stage Sub-Kelvin 3He Cooler No. CRC GL10-001 Installation and Operating Instructions," (Chase Research Cryogenics LTD, Sheffield, UK, 2011).

[7] http://www.lemo.com/.

[8] http://www.eccosorb.com/.

[9] I. Peroni, et al., "Thermal Conductivity of Manganin below 1K," Nuclear Physics B (Proc. Suppl.) **78**, 573-575 (1999).

[10] A. Woodcraft, et al., "The thermal conductivity of C17510 beryllium-copper alloy below 1 K," Cryogenics **41**, 603-606 (2001).

[11] J. W. Ekin, *Experimental Techniques for Low-Temperature Measurements* (Oxford University Press, 2011).

[12] B. G. Gom, "A Cryogenic Detector for Submillimeter Astronomy," (University of Lethbridge, Alberta, Canada, 1999).

[13] http://www.pjrc.com/store/teensypp.html.

[14] http://www.heidenhain.com/.

[15] http://www.mcmaster.com/#5287t32/=vhu91t.

[16] E. D. Marquardt, et al., "Cryogenic Material Properties Database," in *11th International Cryocooler Conference*, Keystone, Co, 2000),

[17] "Torr Seal Low Vapor Pressure Resin Sealant," (Agilent Technologies, 121 Hartwell Avenue, Lexington MA 02421, USA).

[18] R. S. Praveen, et al., "Hybridization of carbon–glass epoxy composites: An approach to achieve low coefficient of thermal expansion at cryogenic temperatures," Cryogenics **51**, 95-104 (2011).

[19] http://www.kaptontape.com/.

[20] G. L. Pilbratt, et al., "Herschel Space Observatory*," A&A **518**, L1 (2010).

[21] http://www.melexis.com/Current-Sensors/IMC-Hall-Current-Sensor-ICs/CSA-1V-614.aspx.

[22] Tomohiro Yokozeki, Yutaka Iwahori, Shin Ishiwata, Kiyoshi Enomoto, "Mechanical properties of CFRP laminates manufactured from unidirectional prepregs using CSCNT-dispersed epoxy," Composites Part A: Applied Science and Manufacturing, Volume 38, Issue 10, October 2007, Pages 2121-2130.

[23] Abusafieh, Abdel A., et al. "Dimensional stability of CFRP composites for space-based reflectors." International Symposium on Optical Science and Technology. International Society for Optics and Photonics, 2001.